Application of the single-channel, single-energy amplitude and partial-wave analysis method to $K^+\Lambda$ photoproduction

A. Švarc *
Rudjer Bošković Institute, Bijenička cesta 54, P.O. Box 180, 10002 Zagreb, Croatia and Tesla Biotech d.o.o., Mandlova 7, 10000 Zagreb, Croatia

Y. Wunderlich
Helmholtz-Institut für Strahlen- und Kernphysik, Universität Bonn, D-53115 Bonn, Germany

L. Tiator
Institut für Kernphysik, Universität Mainz, D-55099 Mainz, Germany

(Received 22 November 2021; accepted 2 February 2022; published 22 February 2022)

The new single-channel, single-energy partial-wave analysis method based on a simultaneous use of amplitude and partial-wave analysis called AA-PWA, developed and tested on η photoproduction in [Phys. Rev. C **102**, 064609 (2020)] is applied to the $K^+\Lambda$ photoproduction for the center-of-mass energy range of 1625 MeV $< W <$ 2296 MeV. A complete set of multipoles has been created. The advantages of the method have been confirmed and a comparison with the only existing single-energy partial-wave analysis of $K^+\Lambda$ photoproduction given in [Phys. Rev. Lett. **119**, 062004 (2017), Eur. Phys. J. A **53**, 242 (2017)] is presented. We confirm the size and shape of Bonn-Gatchina multipoles, but we do not confirm the unambiguous interpretation of the structure in the M_{1-} multipole as a $N(1880)\frac{1}{2}^+$ resonance. The decisive role of the self-consistency of the world database is emphasized.

DOI: 10.1103/PhysRevC.105.024614

I. INTRODUCTION

Single-channel, singe-energy partial-wave analysis (SC-SE-PWA) has always been of particular interest primarily for experimentalists, but also for theorists. For experimentalists, it seemed to be the most direct way to convert measured data to physically interpretable partial waves, and for theorists it seemed to be the most direct way to test the validity of their theoretical approach. Many attempts have been made to prove the uniqueness of SC-SE-PWA [1] even in the case of a single elastic channel, and they culminated with research by Stefanescu, who has formulated necessary conditions for the uniqueness of SC-SE-PWA in the elastic domain[1] [2]. However, as the search for nucleon resonances basically takes place in the inelastic region, the continuum-ambiguity problem became of utter importance [3]. This discussion has started a long time ago, but has never been completely finished. Recently, this problem was reopened by our group and culminated with the conclusion that each single-channel PWA in the inelastic region is inherently model dependent, as it depends on the free-energy- and angle-dependent continuum ambiguity phase which leaves all observables invariant, but the angular-dependent part of the ambiguity mixes partial waves. Hence this makes the quantum numbers of resonances unidentifiable without additional information [4]. Since the full information on the phase can be obtained only from all possible inelastic channels, it remains undetermined in single-channel models, and the only way to make a single-channel PWA unique is to fix this phase to some known value. Here we have to distinguish the following two subcases: single-channel energy-dependent PWA (SC-ED-PWA) and single-channel energy-independent PWA (SC-SE-PWA). In SC-ED-PWA the phase is automatically determined by the analyticity of the continuous ED model but possibly incorrectly as only one channel is involved, and in SC-SE-PWA it is absolutely free, so we just have to take it over from some theoretical calculation. Observe that the common denominator of both cases is that the analysis is deficient and has to be extended to multiple channels, as fixing the continuum-ambiguity phase is only possible by restoring multichannel unitarity, and that can only be done in analyzing all available channels for this reaction. So, we have to use coupled-channels models, but even there the missing phase can only be at least approximately determined as all possible, open two- and three-body channels are never known.

Here we give a short overview of worldly accepted energy-dependent models of kaon photoproduction, and we stress that the most important ones are those which are done within the framework of coupled-channels formalism as they by definition fix the phase. Starting in the 1980s, kaon photoproduction has been investigated in various energy-dependent

*svarc@irb.hr

[1]The proof of uniqueness requires the multivariate analyticity of the amplitude as a function of two Mandelstam variables.

(ED) approaches, isobar models, Lagrangian models, quark models, Regge models, and more. An overview can be found in Ref. [5]. Most of those early modelings were single-channel analyses, where only the coupling to well-known nucleon resonances provided a weak coupling between different channels. In most cases the overall phase problem was ignored or unknown. Comparing the partial waves of those analyses leads often to very large differences, a very clear case of model dependence. In the 1990s the situation was improved by the development of coupled-channels approaches. Starting from the 2-channel problem $\{\pi N, \gamma N\}$, at low energies the phases were completely determined and unique, as the πN phase shifts are free of ambiguities. This is the result of the well-known Watson Theorem from two-body unitarity. It is strictly valid only up to the $\pi\pi N$ threshold, which nominally opens already in the $\Delta(1232)$ resonance region, however with negligible consequences. Starting around $W = 1300$ MeV, when the broad Roper resonance gets excited, first the P_{11} partial wave shows large violations of the Watson theorem. In eta photoproduction the phase ambiguity becomes evident and it cannot be simply cured by a coupled-channels approach with a trivial extension to three channels, $\{\pi N, \eta N, \gamma N\}$. Many attempts have been undertaken to include the three-body channel $\pi\pi N$, in the simplest cases it has been done by effective two-body channels as σN, $\pi\Delta$, and ρN. Over the years the treatment of the three-body channels have been considerably improved, and currently three coupled-channels models are on the market, ANL-Osaka [6–8], Bonn-Gatchina [9,10], and Jülich-Bonn-GWU [11,12], which carefully treat the three-body channels; however, still more or less in approximate ways. These very elaborate investigations have led to the understanding that partial-wave analyses (PWA) are inherently model dependent and will so probably remain in the future. Furthermore, the more phenomenological Kent State University (KSU) model [13–15] has recently been updated with fits to new experimental data. And finally, also the GWU-SAID approach [16], where nucleon resonances are not explicitly built in but are analyzed afterwards from the obtained partial waves, is regularly updated with new data. This approach is less model dependent: it treats coupled channels in the Chew-Mandelstam K-matrix method. The problem totally collapses when genuine three-body channels are involved (not replacing them with effective two-body channels like in $\pi\pi N$). This is specially emphasized by the point, which was already noted by scattering theorists many years ago: for a channel-space of multiple coupled two- and n-body channels, with $n > 2$, unitarity can *only* be used as a tool to model independently and uniquely determine the amplitudes of all possible reactions (including their overall phases) if complete sets of data are given for *all* possible reactions. However, reactions with $n > 2$ particles in the initial state cannot be measured experimentally. Therefore, at least some residual model dependence will always remain in the partial-wave analyses for baryon spectroscopy, at least as soon as one crosses the $\pi\pi N$-threshold (see for instance Sec. 3 of Ref. [17]). So we have to face and live with the fact that each single-channel PWA is inherently model dependent due to the lack of information on unitarity. So, when we compare different PWAs, we have to match the reaction-amplitude phases first.

Constraining SC-SE-PWA has for decades been done by either fixing some partial waves to values from some theoretical model, or penalizing some or all partial waves to the particular constraining theoretical model. This is the traditional way. A strong step forward was taken by the Karlsruhe-Helsinki group in the 1980s [18] when the problem was raised to the level of reaction amplitudes where phase ambiguities appear. Following the work of Stefanescu [2] on the importance of analyticity in two Mandelstam variables, fixed-t analyticity was introduced in πN elastic scattering. Analyticity in t was achieved using the manifestly analytic Pietarinen decomposition of invariant amplitudes and fitting the free parameters of the decomposition to the data base transformed from $[\mathrm{W}_{\mathrm{fixed}}, \theta]$ coordinates into $[t_{\mathrm{fixed}}, W]$ coordinates,[2] while analyticity in Mandelstam s is enforced by using the traditional partial-wave decomposition. The free continuum-ambiguity phase was predetermined by the choice of starting values in the t-variable minimization. As the reaction-amplitude phase is fairly well known for the elastic scattering, this method resulted in the KH80- and KH84 solutions for elastic πN partial waves [18], which have been accepted and used for decades. The same method was recently revived and applied with great success to pion photoproduction [19,20]. Luckily, in pion photoproduction this phase is for sufficiently low energies linked to the well-determined phase of elastic πN scattering due to Watson's theorem [21]. Therefore, in Refs. [19,20] the authors also do not face the problem of the unknown phase. However, for all other reactions where Watson's theorem breaks down (like η or $K\Lambda$ photoproduction) this is not true, so the phase stays poorly determined, and SC-SE-PWA stays model dependent. Triggered by the fact that the continuum-ambiguity phase in SC method in the inelastic domain has to be constrained in particular for reactions where Watson's theorem breaks down, a new method based on only one, i.e., the Mandelstam s variable has been developed in Ref. [22]. However, in this model we openly acknowledge the problem that the continuum-ambiguity phase is unknown, and from the very start constrain it to a phase of some chosen theoretical coupled-channels model. The rest is very similar to the fixed-t analyticity procedure but restricted to the s channel only. The procedure is a two-step process applied to the same database: the first step consists of an amplitude analysis of the database where the moduli of the reaction amplitudes are fit while the reaction-amplitude phases are fixed to the values of a particular ED coupled-channels model (this eliminates the continuum ambiguity); the second step is a standard truncated partial-wave analysis (TPWA), where the reaction amplitudes are forced to be close to the reaction amplitudes of the first step using penalization techniques. In this way the continuity in energy is ensured through the continuous phase, and continuity in angle is ensured by the TPWA. Let us observe that the proposed method relies on using minimal theory dependence, which is given by fixing the phase only. Unfortunately, this works perfectly well only for the ideal case when all observables are self-consistent. This has been shown in Ref. [23] for a complete set of pseudo-observables

[2]Observables are traditionally analyzed in $[\mathrm{W}_{\mathrm{fixed}}, \theta]$ space

(numeric data) for η photoproduction generated by the ETA-MAID model [24] which are by definition self-consistent. The free phase in unconstrained SC-SE-PWA is replaced by the original ETA-MAID phase, and the continuous generating multipoles were exactly reproduced. Unfortunately, real data are never self-consistent, so when the method is applied to real data some discontinuities in partial waves might appear. Therefore, all scatter of the result is the consequence of experimental errors and data inconsistencies. The method has been developed and tested on a world database of η photoproduction and presented in Ref. [22]. As the results for η photoproduction were stable [22], and the pole content of the obtained solution looked very reasonable [4], in this paper we used this method for the $K\Lambda$ photoproduction reaction where the isospin structure is identical. However, the main advantage of $K\Lambda$ photoproduction is that we have access to results from complementary analyses, to which our results can be compared. First of all, there exists a very confident theoretical coupled-channels ED model by the Bonn-Gatchina group to start with [25]. Second, results of SC-SE-PWA made by the same group are published [26,27], so we have direct numbers to compare our results with. The situation is even more favorable. The Bonn-Gatchina SC-SE-PWA was done in the standard way: only lower partial waves were left free, while all higher partial waves were fixed to the Bonn-Gatchina ED model, while we offer the simultaneous variation of all multipoles within the framework of AA-PWA method. So, results and advantages and disadvantages of both approaches can be directly compared. Third, but not the least important, is that we had access to a full $K\Lambda$ photoproduction database in numeric form from the Bonn-Gatchina web page [25]. So, as all input can be made identical, the benefits of the new approach could be clearly detected. We discuss similarities and differences, and point out the reasons why this is so.

II. THE AA-PWA METHOD

In the AA-PWA method, from the very start we openly accept the fact that the overall continuum-ambiguity phase of the reaction amplitudes in any inelastic SC analysis is by default undetermined because it depends on other channels [4], and we fix it to a phase of some chosen theoretical coupled-channels model. However, let us stress that the way it is done in our paper is only an approximation. The amplitude phases contain two parts: the first part are relative phases which are determined by single- and double-polarization observables, and can be uniquely determined in the SC model,[3] and the second part is the continuum-ambiguity phase which is unknown in any SC approach [22]. In principle, we should only fix the unknown continuum ambiguity phase to a theoretical model. However, as the separation of each reaction-amplitudes phase in relative- and continuum ambiguity part is unknown, we opted to fully fix the phases of all four reaction amplitudes. So, we expect that the model we use will be fairly good, and fit also the nonmeasured spin observables. The rest is very similar to procedures implementing fixed-t analyticity [18–20,28], but restricted to the s channel only. The procedure is a two-step process applied to the same data base: the first step is an amplitude analysis of the database, where the moduli of reaction amplitudes are fit while the reaction-amplitude phases are fixed to the values of a particular ED coupled-channels model (this eliminates the continuum ambiguity); and the second step is a standard truncated partial-wave analysis (TPWA) where the reaction amplitudes are forced to be close to the reaction amplitudes resulting from the first step, using a penalization technique. In this way the continuity in energy is ensured through the continuous phase, and continuity in angle is ensured via the TPWA. All scatter of the result is, hence, the consequence of experimental errors and data inconsistencies, as in Ref. [23] it has been shown that fixing only the phase results in a smooth and unique solution in the case where a self-consistent database has been generated in the form of pseudo observables from a known model. The AA-PWA method has been developed and tested on a world database for η photoproduction, and in details presented in Ref. [22].

For the convenience of the reader, we summarize the essence of the method mostly relying on the text in Ref. [4].

In Ref. [22] we have formulated a single-channel, single-energy partial-wave analysis (SC-SE-PWA) procedure of determining reaction amplitude via fitting scattering data when the number of equations may be less than number of unknown quantities, which combines amplitude- and partial-wave analyses into one logical sequence, and directly from the data generates a set of continuous partial waves using a minimally model-dependent input (AA-PWA). We have demonstrated that by controlling the reaction-amplitude phase and freely varying the reaction-amplitude partial waves, we obtain a continuous solution with far better agreement with the used data base than the original energy dependent (ED) model.

The most standard, classic approach is the one where one penalizes partial waves by requiring that fitted partial waves reproduce the observable $\mathcal{O}$ and are at the same time close to some partial waves taken from a theoretical model:

$$\chi^2(W) = \sum_{i=1}^{N_{\text{data}}} w^i \left[\mathcal{O}_i^{\text{expt}}(W,\theta_i) - \mathcal{O}_i^{\text{theor}}(\mathcal{M}^{\text{fit}}(W),\theta_i)\right]^2 + \lambda_{\text{pen}} \sum_{j=1}^{N_{\text{mult}}} \left|\mathcal{M}_j^{\text{fit}}(W) - \mathcal{M}_j^{\text{theor}}(W)\right|^2, \quad (1)$$

where

$$\mathcal{M} \stackrel{\text{def}}{=} \{\mathcal{M}_0, \mathcal{M}_1, \mathcal{M}_2, \ldots, \mathcal{M}_{N_{\text{mult}}}\}.$$

w_i is the statistical weight and N_{mult} is the number of partial waves (multipoles), $\mathcal{M}^{\text{fit}}$ are fitting parameters, and $\mathcal{M}^{\text{theor}}$ are continuous functions taken from a particular theoretical model (for a detailed outline of how the observables $\mathcal{O}_i$ are

[3]Let us remember that in pseudoscalar meson photoproduction, the four observables $d\sigma/d\Omega$, Σ, T, and P determine the absolute values of the four transversity amplitudes (see Table IV in Appendix A), and the remaining four observables in a complete set determine the three remaining relative phases.

composed in terms of multipoles for pseudoscalar meson photoproduction, see Appendix A). Instead, we use the possibility to make the penalization function independent of a particular model as first formulated in the Karlsruhe-Helsinki πN elastic PWA by Höhler in the mid-1980s [18]. Partial waves which are inherently model dependent are replaced with a penalization function which was constructed from reaction amplitudes which can be in principle directly linked to experimental data without any model in the amplitude-reconstruction procedure. So, Eq. (1) was changed to

$$\chi^2(W) = \sum_{i=1}^{N_{\text{data}}} w^i \left[\mathcal{O}_i^{\text{expt}}(W,\theta_i) - \mathcal{O}_i^{\text{theor}}(\mathcal{M}^{\text{fit}}(W),\theta_i)\right]^2 + \mathcal{P}(W),$$
$$\mathcal{P}(W) = \lambda_{\text{pen}} \sum_{i=1}^{N_{\text{data}}} \sum_{k=1}^{N_{\text{amp}}} \left|\mathcal{A}_k(\mathcal{M}^{\text{fit}}(W),\theta_i) - \mathcal{A}_k^{\text{pen}}(W,\theta_i)\right|^2, \tag{2}$$

where $\mathcal{A}_k$ is the generic name for any of reaction amplitudes (invariant, helicity, transversity, ...). $\mathcal{A}_k(\mathcal{M}^{\text{fit}}(W),\theta_i)$ is the reaction-amplitude value generated by the fitted multipoles, and $\mathcal{A}_k^{\text{pen}}(W,\theta_i)$ is the penalizing function coming from the amplitude analysis. However, one is now facing two challenges: to get reaction amplitudes which fit the data, and also to make them continuous. In the Karlsruhe-Helsinki case [18–20,28], this was accomplished by implementing fixed-t analyticity and fitting the data base for fixed t. So, the first step of the KH fixed-t approach was to create the data base $\mathcal{O}(W)|_{t=\text{fixed}}$ using the measured base $\mathcal{O}(\cos\theta)|_{W=\text{fixed}}$, and then to fit them with a manifestly analytic representation of the reaction amplitudes for a fixed t. Manifest analyticity was implemented by using the Pietarinen decomposition of reaction amplitudes. Then the second step was to perform a penalized PWA defined by Eq. (2) in the fixed-W channel where the penalizing factor $\mathcal{A}_k(\mathcal{M}^{\text{pen}}(W,\theta_i))$ was obtained in the first step in a fixed-t channel. In that way a stabilized SE PWA was performed. This approach was revived recently for SE PWA of ηp and $\pi^0 p$ photoproduction and very recently also for pion photoproduction in full isospin by the Mainz-Tuzla-Zagreb collaboration, and analyzed in detail in Refs. [19,20,28].

We propose an alternative. We also use Eq. (2), but the penalizing factor $\mathcal{P}(W)$ is generated by an amplitude analysis performed in the same fixed-W representation, and not in the fixed-t one. The phase is in our approach openly recognized as undeterminable, and taken over from the chosen coupled-channels ED model. This simplifies the procedure significantly and avoids quite some theoretical assumptions on the behavior in the fixed-t representation.

We also propose a two-step process as in Refs. [4,18,28]:

Step 1 Amplitude analysis of experimental data in fixed-W system to generate penalizing factor $\mathcal{P}(W)$.

Step 2 Penalized PWA using Eq. (2) with the penalization factor from *Step 1*.

And now we are bound to say something about the importance of the reaction-amplitude phase. The continuum ambiguity forbids us from concluding about the correct phase in any single-channel analysis because the loss of probability flux to other channels starts after the first inelastic threshold opens. The only way to solve the continuum ambiguity problem is to reintroduce the unitarity constraint in the context of a coupled-channels formalism. If we pick the phase in a single-channel analysis arbitrarily by hand, we are departing from the genuine "true" phase, the phase in which partial waves do not mix, and we introduce a pole-shift from one partial wave into another via the angular dependent part of the continuum ambiguity (see Refs. [23,29]). However, each coupled-channels model by construction results in the non-pole-mixing solution. Namely, some form of interaction introducing poles is formulated, and the background contribution is included. Then, the data in all channels are simultaneously fit, forcing the phase to be the correct one, and the non-pole-mixing situation is established. Background contributions automatically enforce the phase to be a non-mixing one. It is needless to say that all coupled-channels models should end up with the same phase in the ideal case, but incompleteness of the data forbids that to happen. Therefore, phases of different models [16,30–32] are somewhat different, and we cannot avoid this. However, fixing the phase to the phase of a particular model ensures to obtain the non-mixing pole solution; departure from it automatically enforce pole mixing, so the analytic structure of such a solution is spoiled. So, we can chose a different phase, a phase coming from any model, but it has to be the

TABLE I. Experimental data from CLAS and GRAAL used in our PWA. Note that the observables C_x and C_z are measured in a rotated coordinate frame [35]. They are related to the standard observables $C_{x'}$ and $C_{z'}$ in the center-of-mass (c.m.) frame by an angular rotation: $C_x = C_{z'}\sin(\theta) + C_{x'}\cos(\theta)$ and $C_z = C_{z'}\cos(\theta) - C_{x'}\sin(\theta)$, see Ref. [27].

Obs.	N	$E_{\text{c.m.}}$ [MeV]	N_E	$\theta_{\text{c.m.}}$ [deg]	N_θ	Reference
$d\sigma/d\Omega \equiv \sigma_0$	3615	1625–2295	268	28–152	5–19	CLAS(2007) [35], CLAS(2010) [36]
Σ	400	1649–2179	34	35–143	6–16	GRAAL(2007) [37], CLAS(2016) [38]
T	408	1645–2179	34	31–142	6–16	GRAAL(2007) [37],CLAS(2016) [38]
P	1597	1625–2295	78	28–143	6–18	CLAS(2010) [36], GRAAL(2007) [37]
$O_{x'}$	415	1645–2179	34	31–143	6–16	GRAAL(2007) [37], CLAS(2016) [38]
$O_{z'}$	415	1645–2179	34	31–143	6–16	GRAAL(2007) [37], CLAS(2016) [38]
C_x	138	1678–2296	14	31–139	9	CLAS(2007) [35]
C_z	138	1678–2296	14	31–139	9	CLAS(2007) [35]

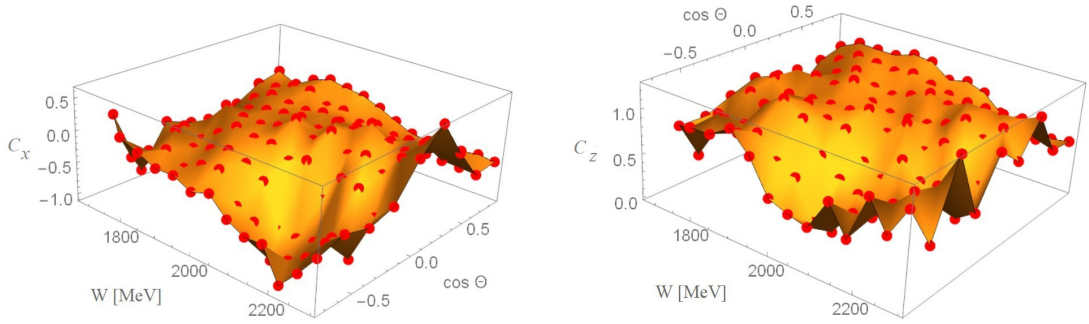

FIG. 1. Quality of the 2D interpolation for C_x and C_z observables. The lighter-hue (red) symbols symbols are measured values, and the lighter-hue (orange) surface shows the interpolated values.

proper phase originating from that model. A free, uncontrolled departure from ED model phase is not allowed.

Of course the question is purely quantitative: How much can we depart from the true phase in an uncontrolled way to maintain the correct analytic properties? In other words, the question is how much we are allowed to reduce the importance of the penalty function and maintain the correct analyticity.

All relevant formulas and more details on the photoproduction formalism are given in Appendix A of this paper.

III. APPLICATION OF AA-PWA to $K^+\Lambda$ PHOTOPRODUCTION DATA

Given that the AA-PWA method worked so well on η photoproduction, we decided to test it on the next natural candidate reaction, and that is $K^+\Lambda$ photoproduction. This reaction has the same isospin structure as η photoproduction, it has a rich database, so the technical effort involved in adapting the AA-PWA scheme was minimal. However, there is one big advantage: we have results from other complementary analyses to compare with. Namely, four years ago the Bonn-Gatchina group made a classic SC-SE-PWA analysis of $K^+\Lambda$ photoproduction. In Ref. [26], the first four multipoles (E_{0^+}, M_{1^-}, E_{1^+}, and M_{1^+}) were let free, while all higher multipoles were forced by a penalty function to stay close to the Bonn-Gatchina ED theoretical coupled-channels model, while in the forthcoming Ref. [27] the next three multipoles (E_{2^-}, M_{2^-}, and M_{2^+}) were released in addition. In this paper we focus on comparing our results with the results of Ref. [26].

However, to do so we have to use the identical data base, and identical Bonn-Gatchina (BG) ED model constraining partial waves. This turned out not to be a problem, as the data base is in numerical form given on two very nice web pages [25,33]. Unfortunately, choosing BG ED multipoles turned out to be much more difficult. For some reason, the particular BG ED solution used for both BG publications [26,27] is not given on the BG web page, so we obtained these numbers via private communication [34]. As the reader will see later, this turned out to be extremely important because this solution was especially tuned to fit $K^+\Lambda$ data, and the absolute normalization of all multipoles is somewhat different. This is trivially

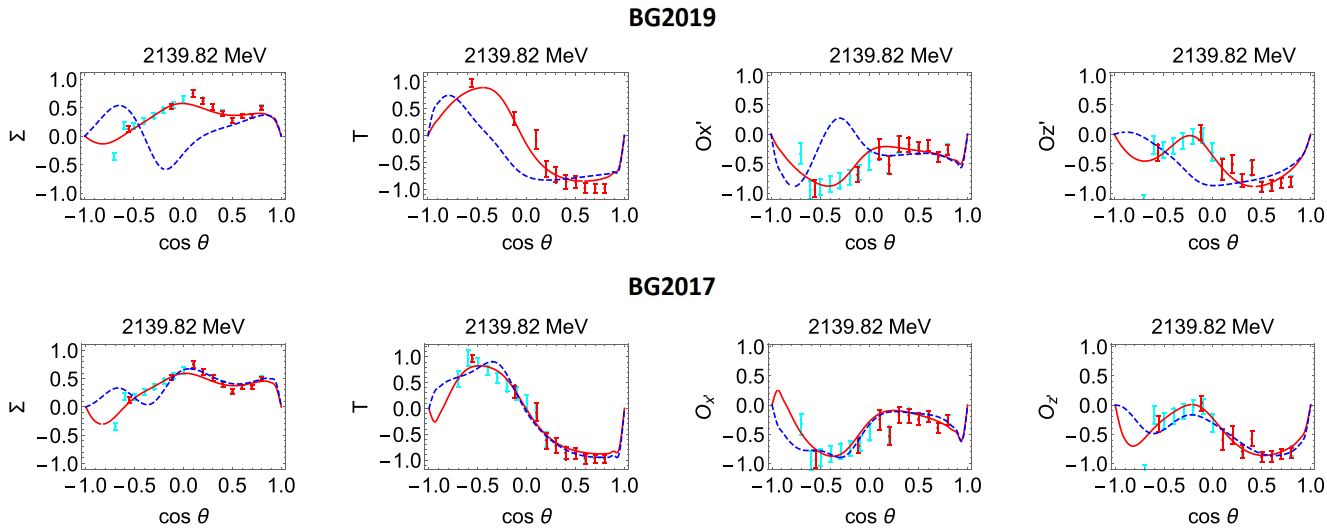

FIG. 2. The quality of the BG2017 and BG2019 solutions for the polarization observables Σ, T, $O_{x'}$, and $O_{z'}$ is illustrated at one randomly chosen energy. Discrete symbols (red) are measured data, light-hue (cyan) symbols are interpolated data, the dashed line (blue) is the result of the BG2019 and BG2017 model respectively, and the full line (red) is the result of our fit.

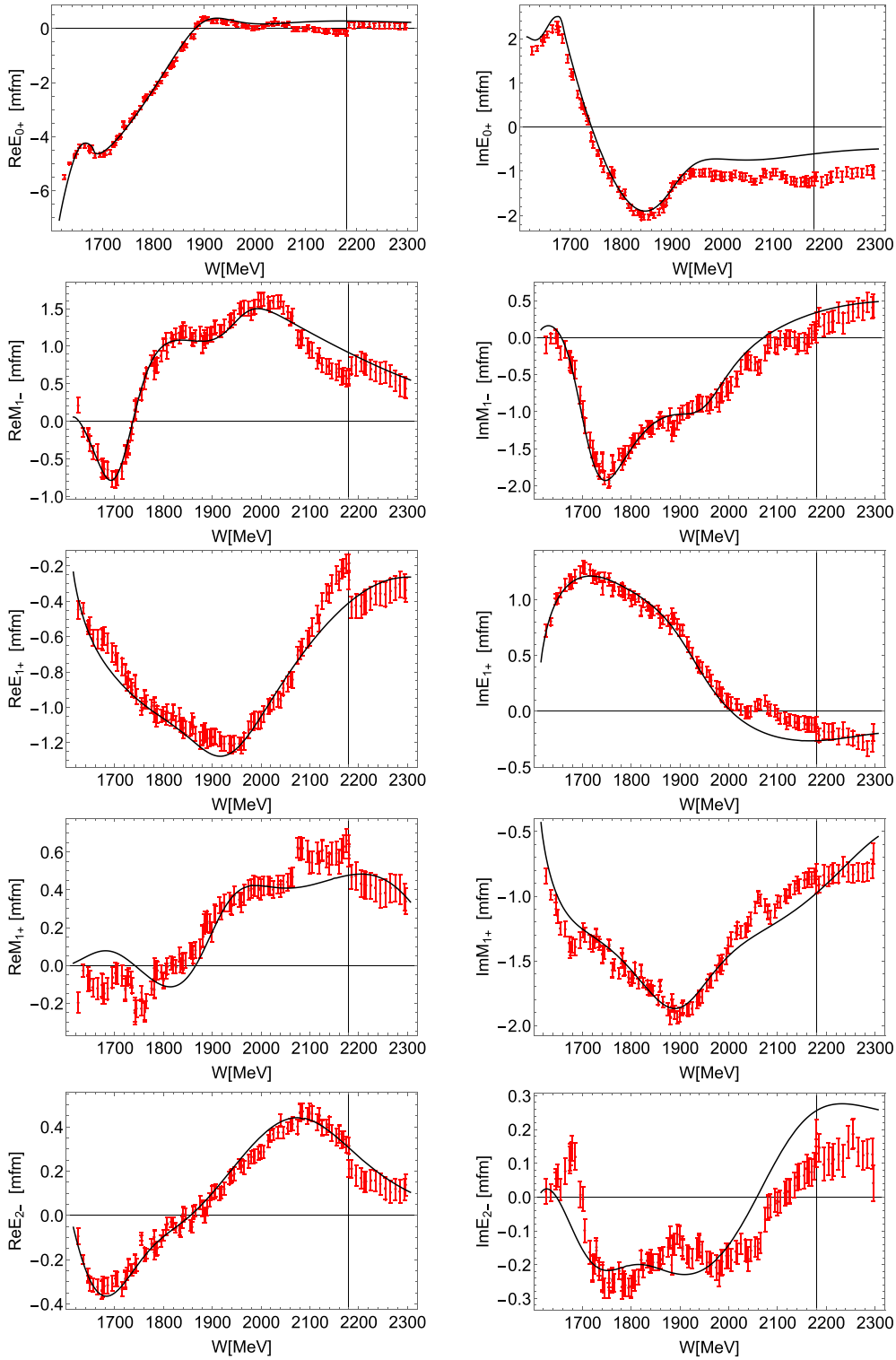

FIG. 3. The multipoles for the $L = 0$, 1, and 2 partial waves of our AA-PWA solution are shown. Red discrete symbols correspond to our solution, and the black full line gives the BG2017 ED solution for comparison. The thin vertical black line marks the energy where only four observables are measured instead of eight (cf. Table I).

visible for the dominant E_{0^+} multipole, where the value of used BG ED solution was notably larger than either of the solutions BG2014-2 or BG2019 given on their web page.

A. Description of the database

In Table I we give our data base which is in numeric form taken over from the Bonn-Gatchina and George Washington

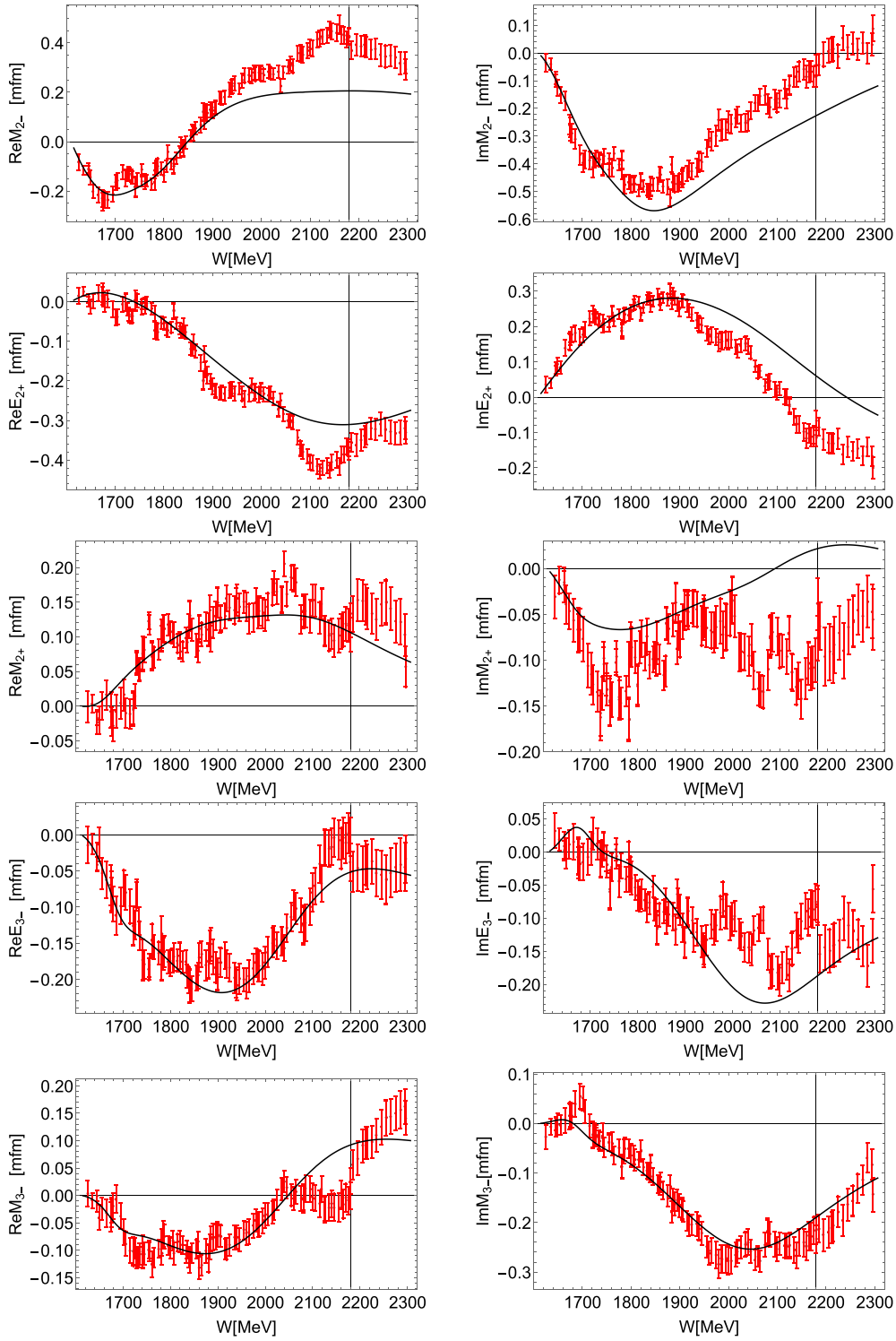

FIG. 4. The multipoles for the $L = 2$ and 3 partial waves of our AA-PWA solution are shown. Red discrete symbols correspond to our solution, and the black full line gives the BG2017 ED solution for comparison. The thin vertical black line marks the energy where only four observables are measured instead of eight (cf. Table I).

University web pages [25,33]. As we see from the Table I, we have a situation at hand which is very similar to η photoproduction:

(1) We have eight measured observables at our disposal, and unfortunately, identically as in η photoproduction, this is still not a complete set of observables

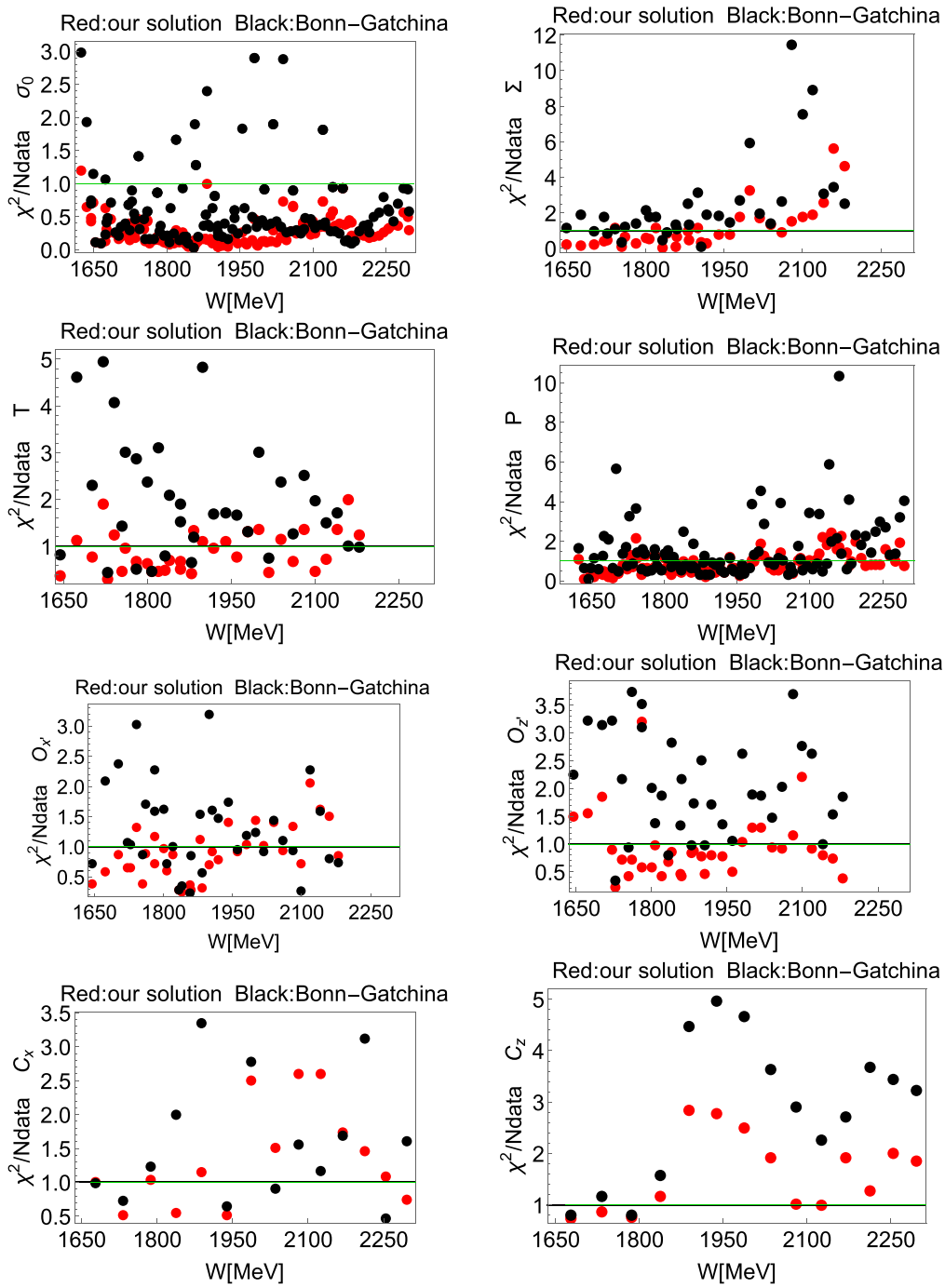

FIG. 5. The χ^2/N_{data} for individual observables, calculated on measured values of energies and angles, is shown. Our AA-PWA solution is given with lighter-hue (red) symbols, and the same quantity evaluated for the ED BG2017 solution [25] is given with black symbols.

(some observables from either the beam-target or the target-recoil categories are missing). For details, see Appendix B 1.

(2) We have a strong dominance of $d\sigma/d\Omega$ data over all other observables.

(3) Only four observables out of eight are given in the full, analyzed energy range of 1625 MeV $< W_{\text{c.m.}} <$ 2296 MeV, and these are $d\sigma/d\Omega$, P, C_x, and C_z. The remaining four observables Σ, T, $O_{x'}$, and $O_{z'}$ are measured only up to ≈2180 MeV. This might create unwanted discontinuities at this energy.[4] For details see Appendix B 2.

[4]Eight observables at lower energies might create slightly different multipoles than only four at energies above ≈2180 MeV. So, the transition may not be smooth for all multipoles at this energy.

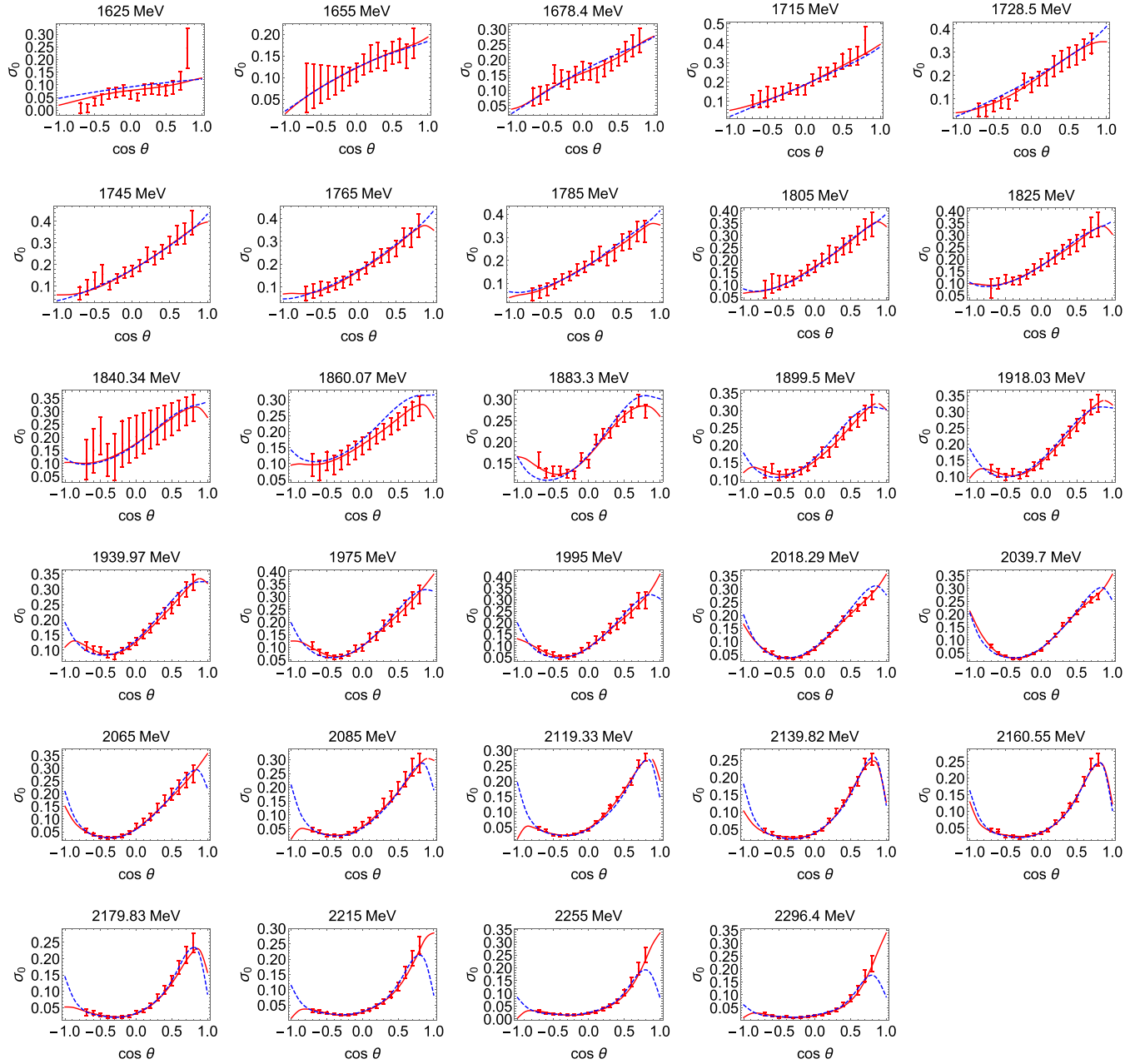

FIG. 6. Comparison of experimental data for σ_0 (discrete symbols) with our results from AA-PWA full line (red) and the BG2017 fit dashed line (blue) at representative energies.

Even a superficial glimpse at Table I tells us that the measured data are given at different energies and different angles, so some data rebinning is in order. Standardly, data binning consists of using the data not at the exact energy where they were taken, but in the energy interval $W_{\text{exact}} - \Delta/2 < W_{\text{exact}} < W_{\text{exact}} + \Delta/2$, where Δ is the energy bin width. However, in the case of scarce data this procedure might introduce an unwanted dissipation of data, resulting in possible discontinuities between energy bins. Therefore, we have adopted and used an altogether different method. Instead, we rely on a two-dimensional (2D) data interpolation. We simultaneously interpolate experimental data and their corresponding experimental error in energy W and angle θ using a standard *Mathematica* routine [39], and use interpolated values instead of binned ones.

Our interpolation strategy is as follows:

(i) *Energy grid.* The analysis is performed on a collection of energies where at least one polarization observable apart from the cross section σ_0 was measured (141 energy points).

(ii) *Angular grid.* The analysis is done on the following prechosen fixed values of 16 points: $(\cos\theta) = \{-0.7, -0.6, -0.5, -0.4, -0.3, -0.2, -0.1, 0., 0.1, 0.2, 0.3, 0.4, 0.5, 0.6, 0.7, 0.80\}$.

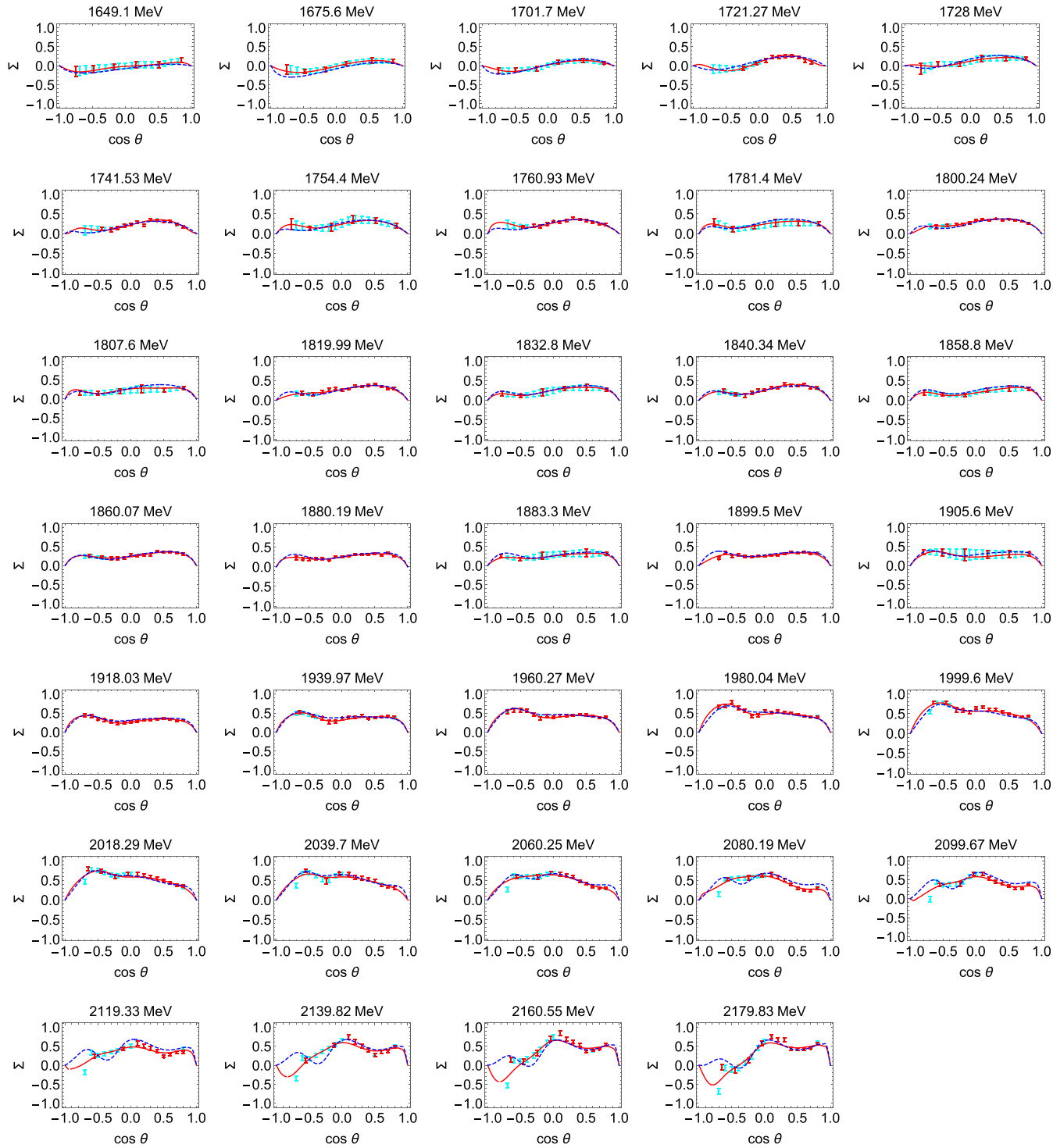

FIG. 7. Comparison of experimental data for Σ (discrete symbols) and interpolated values lighter-hue (cyan) symbols with our results from AA-PWA full line (red) and the BG2017 fit dashed line (blue) at representative energies.

So, let us summarize. The AA-PWA method is not done on the realistic, measured energy and angular values, but at interpolated values of all observables instead. Instead, some interpolation has to be done since we are doing a single-energy analysis, i.e., at least energies between analyzed observables have to match (which they do not do for the measured data sets). This has some advantages and possibly some drawbacks. The main advantage is that the number of analyzed points is increased. In the standard binning method, the number of analyzed energy and angular points is directly limited by the number of measured points for the least known observable. So, when we perform the analysis with the energy-binning technique, we can make an analysis using a maximum number of observables only on a small number of

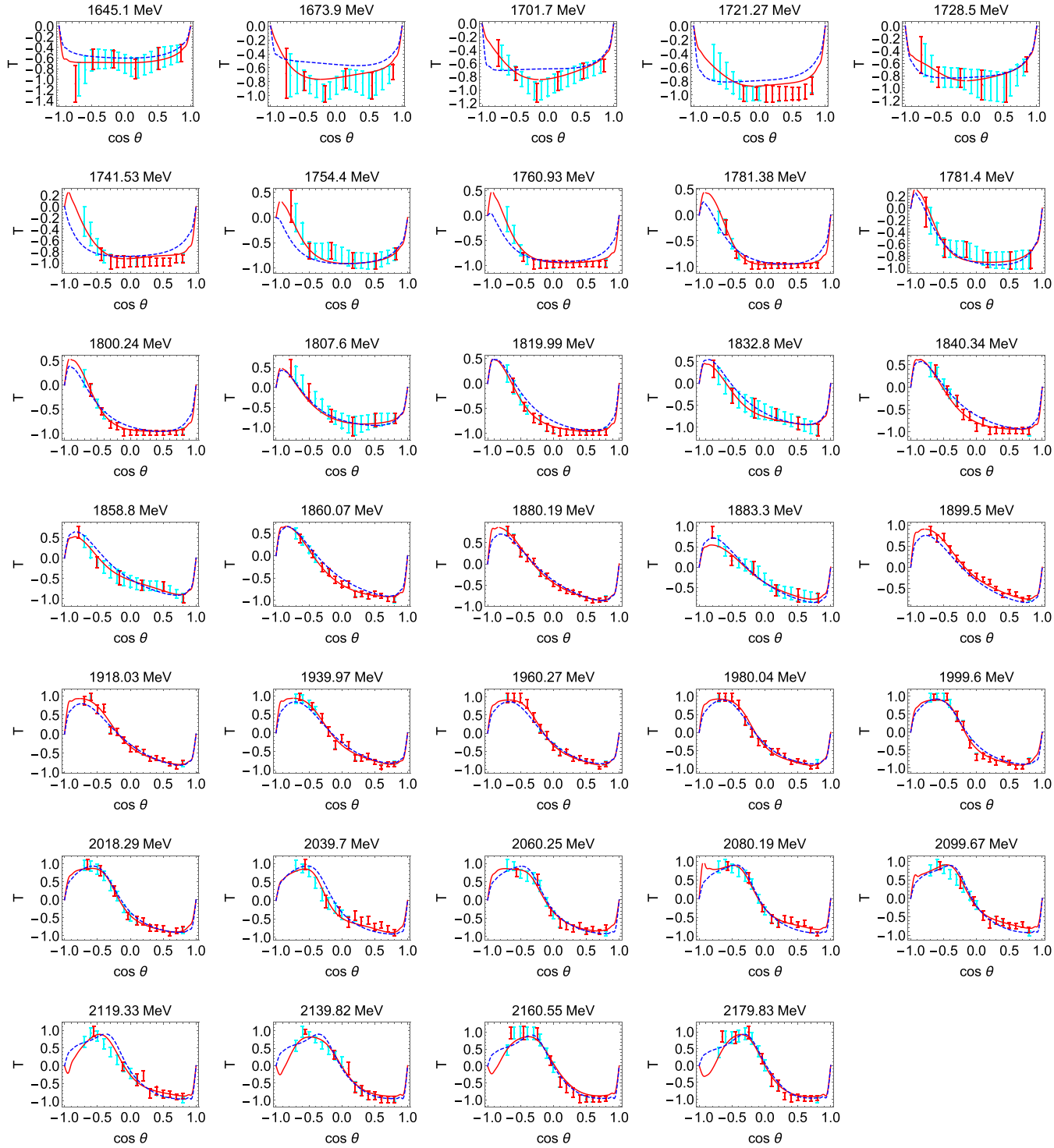

FIG. 8. Comparison of experimental data for T (discrete symbols) and interpolated values lighter-hue (cyan) symbols with our results from AA-PWA full line (red) and the BG2017 fit dashed line (blue) at representative energies.

points, on points where the least known observable is measured. We can never benefit from the vast amount of energy and angular points where all other energies are measured. On the rest of the energies and angles the number of used observables is smaller, and the uncertainty introduced into the analysis hence grows. However, when we use the interpolation technique, we have all measured observables at all analyzing points as interpolated values, and the confidence into our analysis depends on the quality of the interpolation. So, it is of utter importance to have a confident interpolation for the "worst" observable where the separation between measured points is the farthest. In our case the worst observables are C_x

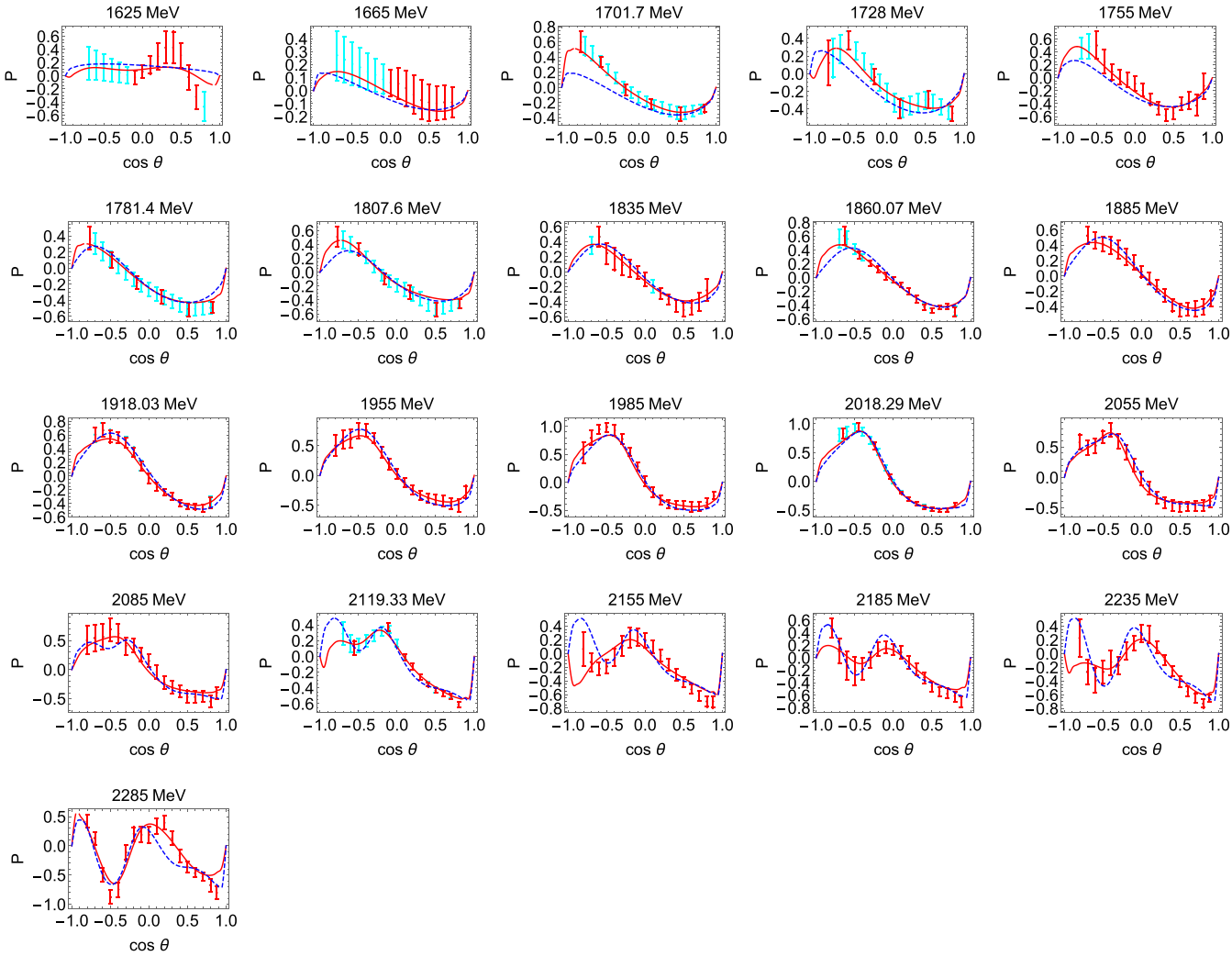

FIG. 9. Comparison of experimental data for P (discrete symbols) and interpolated values lighter-hue (cyan) symbols with our results from AA-PWA full line (red) and the BG2017 fit dashed line (blue) at representative energies.

and C_z (see Table I), and in Fig. 1 we show the quality of the corresponding interpolations. We are of the opinion that the interpolation of these two observables is fairly good.

Of course, the natural drawback is that we introduce additional unmeasured points, so the contribution of poorly measured observables to the overall χ^2 grows. However, this effect of over-stressing the statistical importance of poorly measured observables is present in the binning technique, but is introduced differently (by increasing the weighting factor for these observables). So, the idea is similar, but for the interpolation method implemented in a more confident way.

Our fitting strategy reads as follows:

(i) The AA step is done on interpolated energies (141 points) and interpolated angles (16 points).
(ii) The TPWA minimization step for obtaining multipoles is also done on interpolated energies and prechosen angular values. However, the statistical data analysis to obtain χ^2 is done at exact energies and exact number of angles (energy dependent) for each observable (cf. Table I).

B. Choosing the energy-dependent constraining model

Our first intention was to take the solution BG2019 from the Bonn-Gatchina web page [25] as a constraining solution. To our surprise, this solution fits the polarization observables Σ, T, $O_{x'}$, and $O_{z'}$ rather poorly at higher energies. We show the discrepancy of that solution with the above-mentioned four observables at one randomly chosen higher energy in Fig. 2. However, when the SE-PWA has been performed in Refs. [26,27], another Bonn-Gatchina ED model was used to constrain the higher partial waves, and this solution was different from BG2019. We call this solution the BG2017 model. As one of the goals of the present paper is to compare the results of our AA-PWA method with results from Bonn-Gatchina publications, it is natural to take the same constraining input, but to be used on the level of reaction-amplitude phases. As seen in Refs. [26,27] the agreement of the BG2017 model with polarization observables is very good, and this is very important for choosing the phase as we fix relative phases in addition to the continuum-ambiguity phase. Unfortunately, we realized that this solution is never given anywhere in numbers

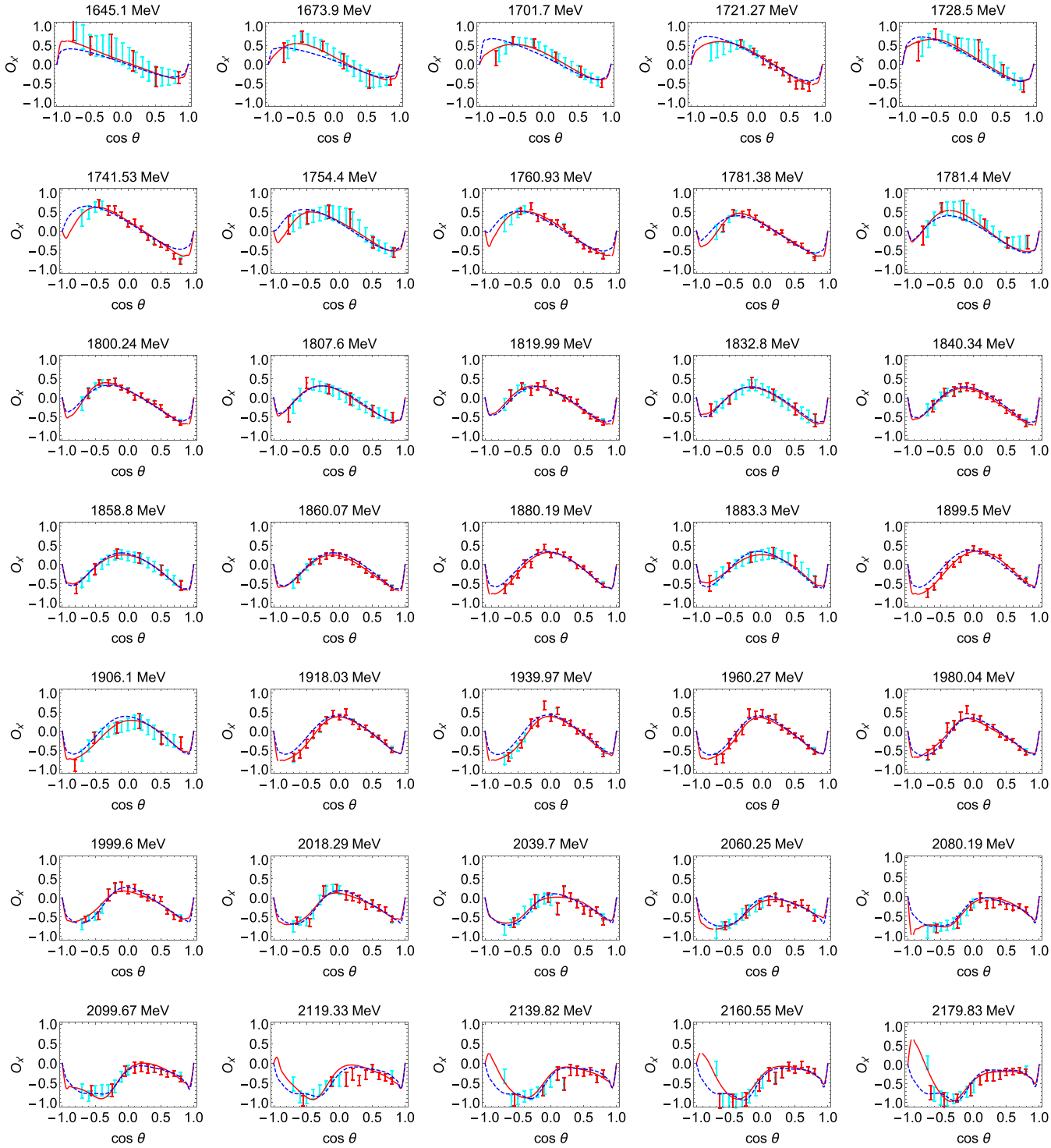

FIG. 10. Comparison of experimental data for $O_{x'}$ (discrete symbols) and interpolated values (cyan symbols) with our results from AA-PWA (red full line) and the BG2017 fit (blue dashed line) at representative energies.

explicitly, and we got it only via private communication [34]. As our model requires fairly good agreement with all data, the natural model of choice for the constraining phase had to be the officially unpublished BG2017 model, in spite of the fact that it is older and actually never published.

C. Results

In Figs. 3 and 4 we show our final results for multipoles on the full set of energies. The penalty factor λ is picked by hand and is set to $\lambda = 250$. Red symbols give the values of multipoles for our AA-PWA solution, and the

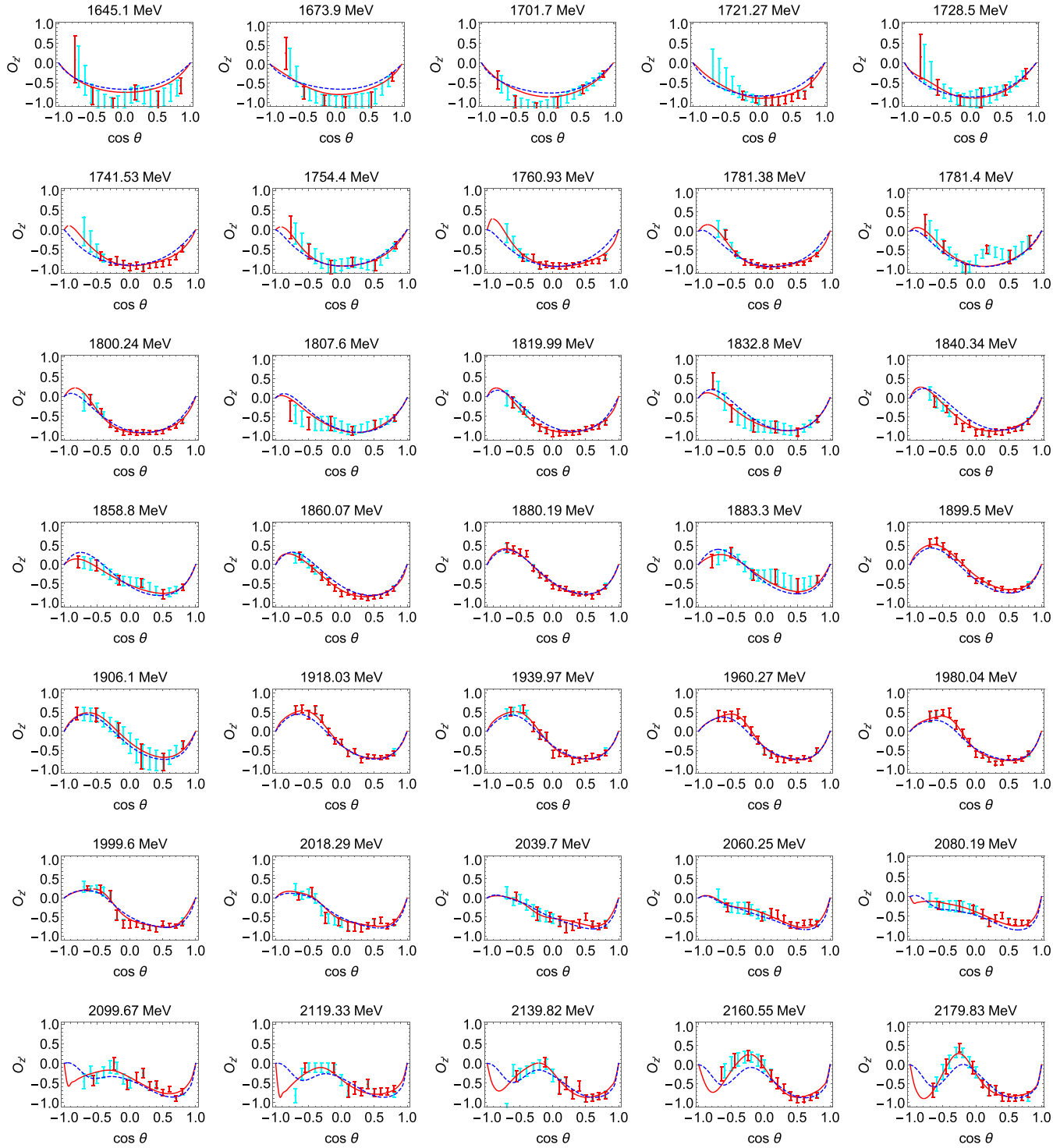

FIG. 11. Comparison of experimental data for $O_{z'}$ (discrete symbols) and interpolated values (cyan symbols) with our results from AA-PWA (red full line) and the BG2017 fit (blue dashed line) at representative energies.

black full line gives the prediction of the BG2017 solution [25]. In Fig. 5 we give the χ^2 per data point for each observable calculated on measured values of energies and angles as red symbols, and the same quantity for the ED BG2017 solution [25] as black symbols. In Figs. 6–13 we give the fits to measured observables resulting from our AA-PWA method (red full line) as well as predictions from the ED BG2017 solution [25] (dashed blue line) at representative energies only. All further energies are available upon demand.

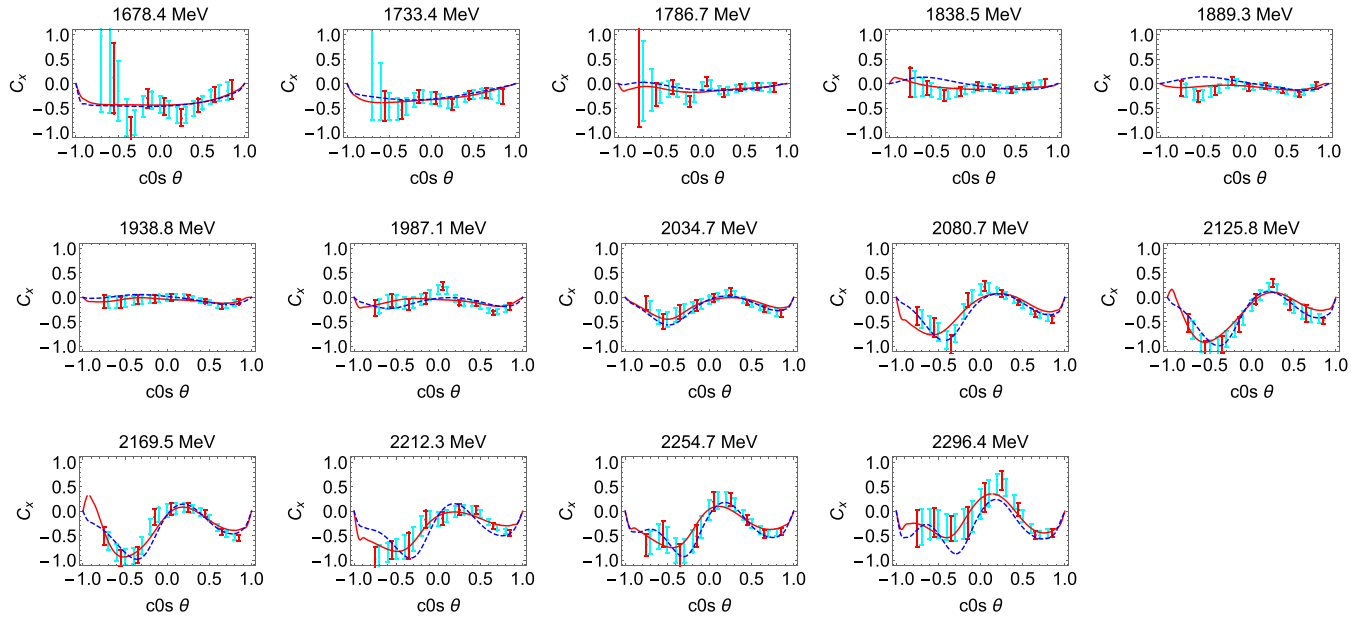

FIG. 12. Comparison of experimental data for C_x (discrete symbols) and interpolated values (cyan symbols) with our results from AA-PWA (red full line) and the BG2017 fit (blue dashed line) at representative energies.

In Fig. 14 we also give predictions resulting from our AA-PWA method for the unmeasured $\mathcal{BT}$ polarization observables E, F, G, and H at two representative energies out of the full energy range.

We have also given predictions for unmeasured $\mathcal{BT}$ observables E, F, G, and H. They show good agreement at low energies and larger spread at the highest energies. This is, however, also already seen in the $\mathcal{BR}$ observables that are fitted. Many observables shown in the paper, like T, show sharp structures near 0° and 180°, especially for higher energies. We consider those structures as natural, since most observables must vanish at those extreme angles, either as $\sin(\theta)$ or $\sin^2(\theta)$. And at higher energies, when lots of multipoles can contribute, the bending towards zero becomes quite sharp. In the experiment such structures are hard to see because of the small solid angles.

Up to about 2 GeV the fitted data are practically complete, and further additional polarization observables will hardly improve the PWA. Above 2 GeV and even more above 2.2 GeV, the number of observables and also the quality of the data is

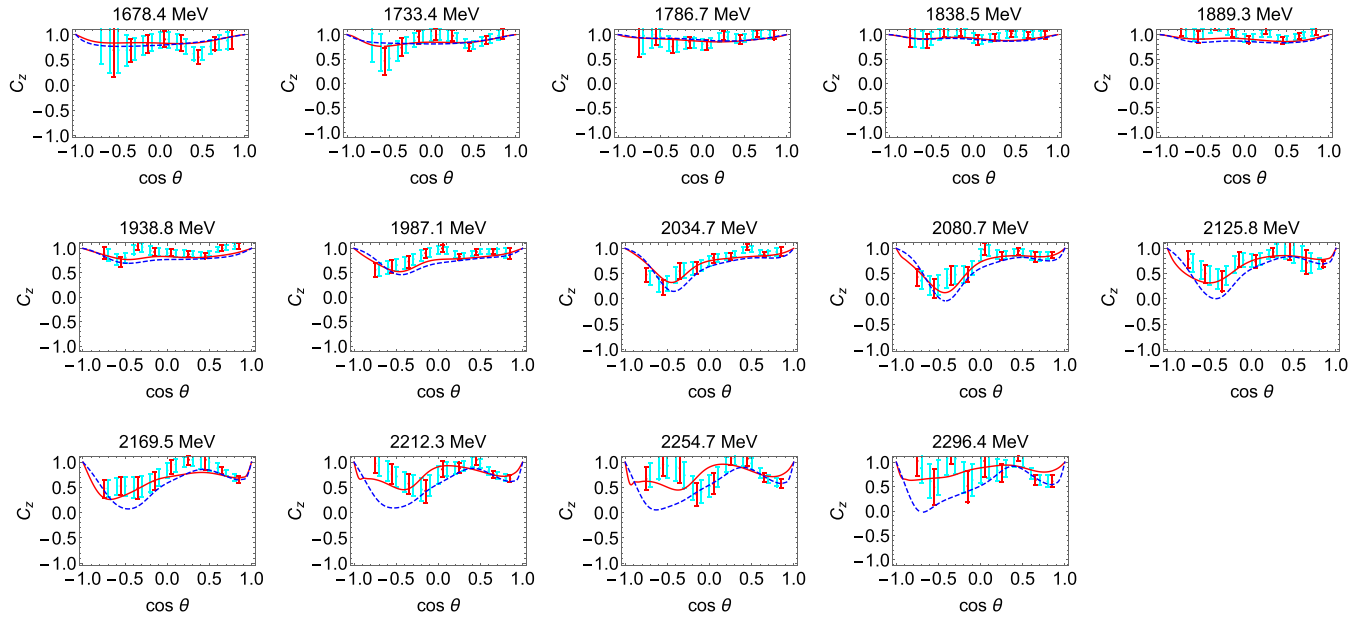

FIG. 13. Comparison of experimental data for C_z (discrete symbols) and interpolated values (cyan symbols) with our results from AA-PWA (red full line) and the BG2017 fit (blue dashed line) at representative energies.

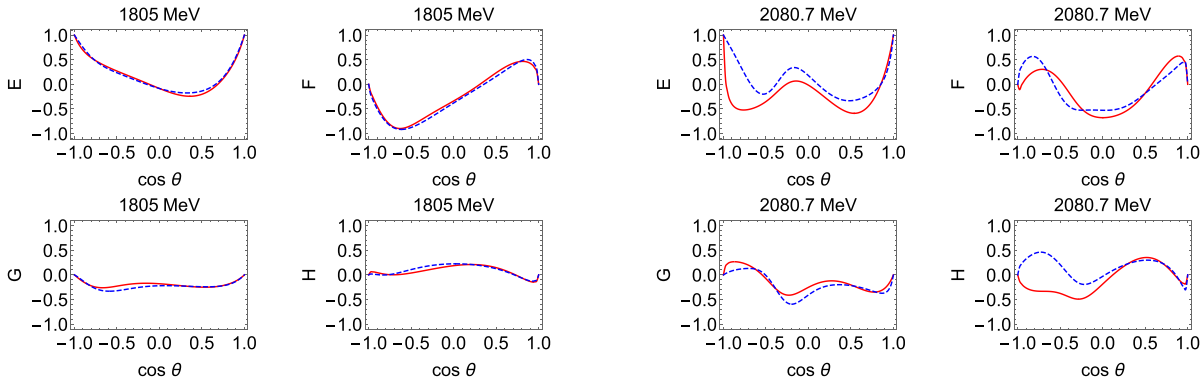

FIG. 14. Prediction of our AA-PWA method full line (red) and the BG2017 fit dashed line (blue) for the E, F, G, and H spin observable at the representative energies of $W = 1805$ and $W = 2080.7$ MeV out of the full energy range.

more limited and additional measurements of $\mathcal{BT}$ observables can very well improve the PWA.

D. Discussion

The obtained multipoles given in Figs. 3 and 4 are very close to the values of the chosen theoretical model BG2017. This demonstrates the stability of that model; however, some additional resonant structures in all multipoles are made more visible which is to expected as the AA-PWA is significantly improving the ED BG2017 fit for all observables in the particular channel of $K\Lambda$ photoproduction, see Fig. 5.

The AA-PWA multipoles are fairly smooth. However, we would like to warn the reader that we basically have two distinct energy ranges: the lower one where eight observables have been measured (1625 MeV $< W <$ 2179 MeV), and the higher one where only four observables have been measured (2179 MeV $< W <$ 2296 MeV). As fits are in principle done on individual energies one by one, they are correlated only through the penalty function, so a change in multipoles due to the change of the number of observables might be expected (cf. the solution theory discussed in Appendix B). The crucial energy where the transition happens is indicated by the vertical black line at 2179 MeV in all figures. The fits in the lower energy range should tend to be smoother, and more constrained, while some visible changes might occur at higher energies. This produces discontinuities. As the AA-PWA method gives a set of smooth multipoles for a self-consistent and complete dataset by forcing the reaction-amplitude phases to be smooth (this has been shown in Ref. [23]), this indicates that the remaining discontinuities are the result of an inconsistency of the database. So, the AA-PWA method offers a possibility to test the self-consistency of the experimental database. However, this discussion can be reliably performed only when a confident method for pole detection is used, so one should in principle get some answers with the use of Laurent plus Pietarinen (L + P) formalism [40–43].

E. Comparison of AA-PWA with BG SC-SE-PWA of Ref. [26]

For relatively new methods such as AA-PWA, a comparison with old, double-checked, and worldly accepted models is crucial. Such an opportunity is offered to us by the Bonn-Gatchina group. They have performed SE-PWA and used the standard constrained PWA method (letting lower multipoles free and strongly penalizing higher ones to theoretical ED

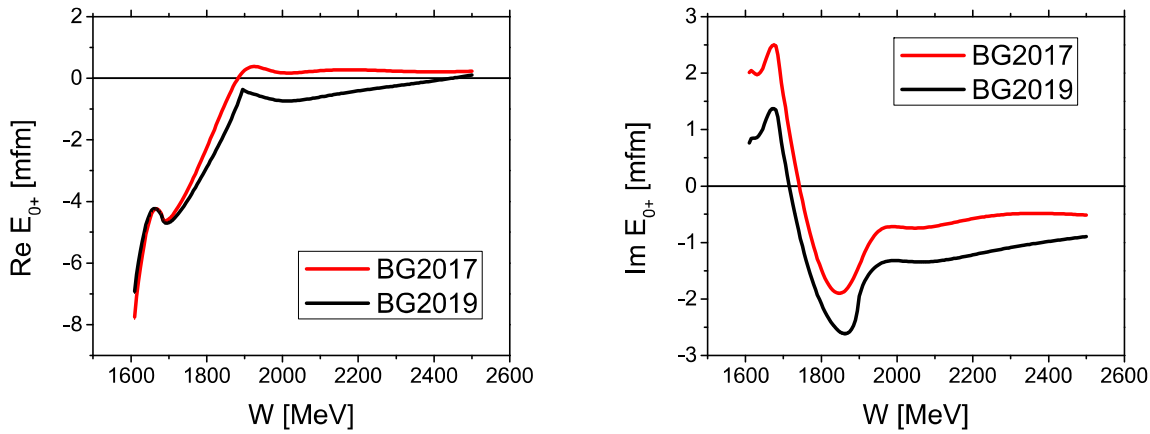

FIG. 15. A comparison of E_{0+} BG ED solution BG2017 from Ref. [26] lighter-hue (red) full line which was used in this publication, and the BG2019 solution given in BG2019 [25] full line (black).

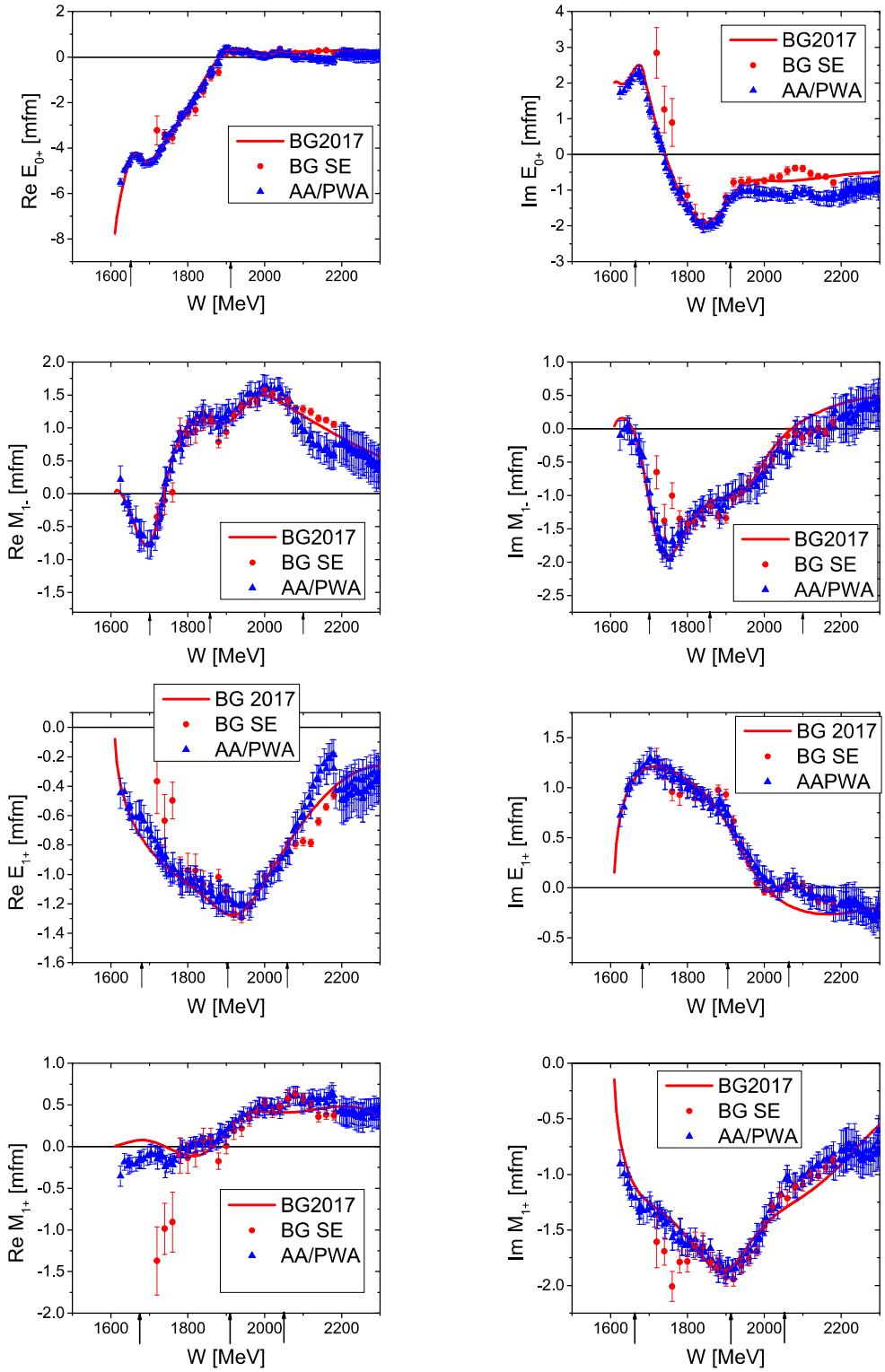

FIG. 16. Comparison of E_{0+}, M_{1-}, E_{1+}, and M_{1+} SC-SE-BG PWA solutions presented in Ref. [26] full circles (red) and the same multipoles obtained using the AA-PWA method in this publication full triangles (blue). The lighter-hue full line (red) is the BG2017 ED solution used in the SC-SE-BG PWA publication, see Ref. [25]. Black arrows on the horizontal axis mark the pole masses of nucleon resonances as given by PDG [44].

values; cf. Sec. II). This enabled us to make a direct comparison of our results with theirs. As we mentioned before, their constraining ED solution was, unfortunately, not made public, but differed notably from the values of the published old BG2014-02 and new BG2019 solutions [25] (we show the difference for the E_{0+} multipole in Fig. 15). However, upon request, they provided us with the exact numbers [34] for all multipoles. So, as our AA-PWA method required exactly the same input (data base and theoretical ED multipoles), and we have achieved that, we used the chance to compare the results directly.

We show in Fig. 16 the result for the four lower multipoles, where the SE results of Ref. [26] only exist. We see a very good agreement between both solutions regarding the overall absolute values and functional shape. Both solutions are also quite close to the constraining BG2017 ED solution.

We see that the AA-PWA method results in many more points. This is a result of the data-preparation philosophy because the AA-PWA method uses data interpolation instead of data binning as the Bonn-Gatchina SE-PWA does.

We see some discrepancy in the absolute values of some multipoles at lower energies, but our values are closer to the BG2017 values. We conclude that both SE methods are in full agreement.

The advantage of the AA-PWA method is obvious: first we generate much many more data points in reconstruction multipoles, and second we generate all multipoles, and not only the lowest ones.

The main issue is to answer the question whether we reproduce the structures in the M_{1-} multipole around 1890 MeV, which were interpreted in Ref. [26] as a confirmation of the $N(1880)\frac{1}{2}^+$ resonance. The answer is definitely affirmative: Yes, we do. However, the "size" of the structure is not so pronounced, so we need a detailed L + P analysis to confirm or dismiss this interpretation. This will be done in the forthcoming section of this paper.

IV. EXTRACTION OF RESONANCE PARAMETERS FROM THE SINGLE-ENERGY MULTIPOLES

Extracting poles directly from SE partial-wave solutions is very difficult, and the only method which showed quite some flexibility and confidence is the L + P method [40–43]. So we use this method to analyze the crucial multipole M_{1-}. However, for the convenience of the reader, we repeat the essence of the method in Sec. IV A.

A. The L + P method

The driving concept behind the Laurent-Pietarinen expansion (L + P) was the aim to replace elaborate theoretical models by a local power-series representation of partial-wave amplitudes [41]. The complexity of any reaction-theoretical model which leads to partial waves is thus replaced by a much simpler model-independent expansion which just exploits analyticity. The L + P approach separates the pole and regular parts in the form of a Laurent expansion, and instead of modeling the regular part by some physical model it uses a conformal mapping to expand it into a rapidly converging power series with well-defined analytic properties. In such an approach the model dependence is minimized and is reduced to the choice of the number and location of branch points used in the L + P expansion.

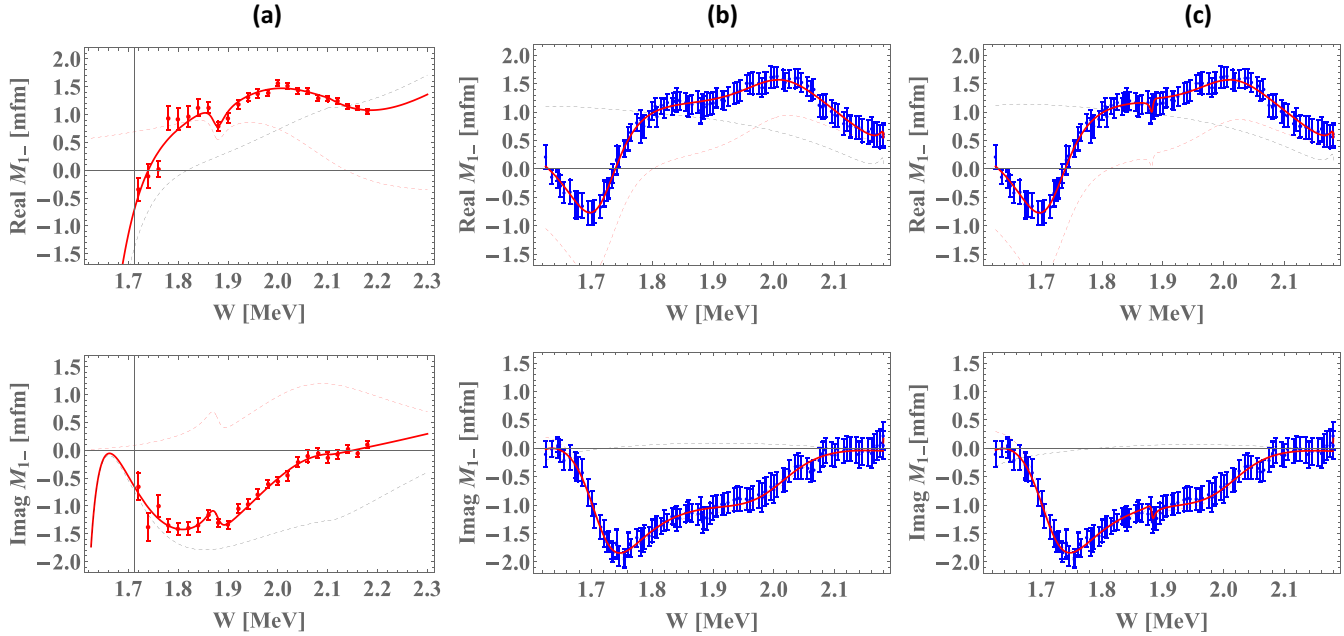

FIG. 17. The L + P fit of the M_{1-} multipole. In panel (a) we show the result of the single-channel fit of BG-SE data, in panel (b) we show the result of the two-pole fit of our AA-PWA solution, and in panel (c) we show the result of its three-pole fit. Red and blue symbols are single-energy BG-SE and AA-PWA solutions, the thin dashed red line is the resonant contribution, thin dashed black line is the background part, and thick red line is the result of the full fit.

TABLE II. Formulas defining the Laurent plus Pietarinen (L + P) expansion (see Ref. [27]).

$$T^a(W) = \sum_{j=1}^{N_{pole}} \frac{x_j^a + iy_j^a}{W_j - W} + \sum_{k=0}^{K^a} c_k^a X^a(W)^k + \sum_{l=0}^{L^a} d_l^a Y^a(W)^l + \sum_{m=0}^{M^a} e_m^a Z^a(W)^m$$

$$X^a(W) = \frac{\alpha^a - \sqrt{x_P^a - W}}{\alpha^a + \sqrt{x_P^a - W}}, \quad Y^a(W) = \frac{\beta^a - \sqrt{x_Q^a - W}}{\beta^a + \sqrt{x_Q^a - W}}, \quad Z^a(W) = \frac{\gamma^a - \sqrt{x_R^a - W}}{\gamma^a + \sqrt{x_R^a - W}}$$

$$D_{dp}^a = \frac{1}{2N_W^a - N_{par}^a} \sum_{i=1}^{N_W^a} \left\{ \left[\frac{\mathrm{Re}T^a(W^{(i)}) - \mathrm{Re}T^{a,exp}(W^{(i)})}{\mathrm{Err}_{i,a}^{\mathrm{Re}}} \right]^2 + \left[\frac{\mathrm{Im}T^a(W^{(i)}) - \mathrm{Im}T^{a,exp}(W^{(i)})}{\mathrm{Err}_{i,a}^{\mathrm{Im}}} \right]^2 \right\} + \mathcal{P}^a$$

$$\mathcal{P}^a = \lambda_c^a \sum_{k=1}^{K^a} \left(c_k^a\right)^2 k^3 + \lambda_d^a \sum_{l=1}^{L^a} \left(d_l^a\right)^2 l^3 + \lambda_e^a \sum_{m=1}^{M^a} \left(e_m^a\right)^2 m^3, D_{dp} = \sum_{a}^{all} D_{dp}^a$$

a is the channel index. N_{pole} is the number of poles. $W_j, W \in \mathbb{C}$.

$x_i^a,\ y_i^a,\ c_k^a,\ d_l^a,\ e_m^a,\ \alpha^a,\ \beta^a,\ \gamma^a \in \mathbb{R}$

$K^a,\ L^a,\ M^a \in \mathbb{N}$ are the number of Pietarinen coefficients in channel a.

D_{dp}^a is the discrepancy function in channel a. N_W^a is the number of energies in channel a.

N_{par}^a is the number of fitting parameters in channel a. $\mathcal{P}^a$ is the Pietarinen penalty function.

$\lambda_c^a, \lambda_d^a, \lambda_e^a$ are the Pietarinen weighting factors. $x_P^a,\ x_Q^a,\ x_R^a \in \mathbb{R}$ (or $\in \mathbb{C}$).

$\mathrm{Err}_{i,a}^{\mathrm{Re}}$ and $\mathrm{Err}_{i,a}^{\mathrm{Im}}$ are the minimization error of the real and imaginary parts, respectively.

The L + P expansion is based on the Pietarinen expansion used in some older papers in the analysis of pion-nucleon scattering data [45–48], but for the L + P model the Pietarinen expansion is applied in a different manner. It exploits the Mittag-Leffler theorem[5] of partial-wave amplitudes near the real energy axis, representing the regular, but unknown, background term by a conformal-mapping-generated, rapidly converging power series called a Pietarinen expansion.[6] The method was used successfully in several few-body reactions [40,42,43] and was recently generalized to the multichannel case [50]. The formulas used in the L + P approach are collected in Table II.

In the fits, the regular background part is represented by three Pietarinen series and all free parameters are fitted. The first Pietarinen expansion with branch point x_P is restricted to an unphysical energy range and collectively represents all left-hand singularities. The next two Pietarinen expansions describe the background in the physical energy range with branch points x_Q and x_R respecting the analytic properties of the analyzed partial wave. The second branch point is in most cases fixed to the elastic channel branch point, the third one is either fixed to the dominant inelastic threshold, or left free. Thus, only rather general physical assumptions about the analytic properties are made like the number of poles and the number and the position of branch points, and the simplest analytic function with the correct set of poles and branch points is constructed. The method is applicable to both, theoretical and experimental input, and represents a reliable procedure to extract pole positions from experimental data, with minimal model bias.

The generalization of the L + P method to a multichannel L + P method is performed in the following way: (i) separate Laurent expansions are made for each channel; (ii) pole positions are fixed for all channels, (iii) residues and Pietarinen coefficients are varied freely; (iv) branch points are chosen as for the single-channel model; (v) the single-channel discrepancy function D_{dp}^a [see Eq. (5) in Ref. [40]] which quantifies the deviation of the fitted function from the input is generalized to a multichannel quantity D_{dp} by summing up all single-channel contributions; and (vi) the minimization is performed for all channels in order to obtain the final solution.

B. Detailed analysis of the M_{1-} multipole using the L + P method

The only reliable way to establish whether the structure seen in the M_{1-} multipole corresponds to a resonance pole is to use the L + P formalism, and try to find any analytic function with an explicit pole and realistic background which fits the data. If we find it, then we can claim that the observed structure is at least consistent with a function having a pole. Very often, especially for narrow or small resonances, such a function cannot be found, so this is an indication that the observed structure is originating not from a pole, but from some other effect possible in the method.

In Ref. [26] the L + P formalism was used to analyze the obtained result, and it was found that a function containing a pole of mass $M = 1876$ MeV and a width of $\Gamma = 33$ MeV can describe the data well, so in spite of the fact that the width was rather narrow for the formerly found state $N(1880)\frac{1}{2}^+$ [33(19) MeV corresponding to previously established 230(50) MeV] it was interpreted as a signal of a new resonant

[5]Mittag-Leffler theorem [49]: This theorem provides the generalization of a Laurent expansion to a more-than-one-pole situation. For simplicity, we simply refer to this as a Laurent expansion.

[6]A conformal-mapping expansion of this particular type was introduced by Ciulli and Fisher [45,46]. It was described in detail and used in pion-nucleon scattering by Pietarinen [47,48]. The procedure was denoted as a Pietarinen expansion by Höhler in Ref. [18].

TABLE III. The pole parameters for the M_{1-} multipole extracted using the single-channel L + P formalism of Refs. [40–43] are given. BG-SE denotes the solution of Refs. [26,27] with one pole, and AA-PWA denotes two solutions for AA-PWA determined in this paper, with two and three poles respectively. M_i, Γ_i, r_i, and θ_i, $i = 1, \ldots, 3$ are pole masses, widths as well as absolute values of the residue and its phase, while χ^2 is the value of the total chi-squared. Values given by the PDG [44] for these resonances are given in bold for comparison.

Model	M_1	Γ_1	$\lvert a_1\rvert$	θ_1	M_2	Γ_2	$\lvert a_2\rvert$	θ_2	M_3	Γ_3	$\lvert a_3\rvert$	θ_3	χ^2
PDG	**1700(40)**	**120(40)**			**1860(40)**	**230(50)**			**2100(50)**	**290(50)**			
BG-SE					1876(11)	31(19)	6(2)	57(14)					36
AA-PWA$^{2\text{poles}}$	1715(12)	118(31)	117(62)	12454(35)					2002(59)	201(100)	84(103)	−116(92)	32.7
AA-PWA$^{3\text{poles}}$	1714(19)	120(33)	122(98)	121(45)	1882(3)	6(6)	0.6(0.6)	123(54)	2007(70)	187(102)	71(120)	−113(108)	29.2

state. Unfortunately, in the present paper we do not confirm this finding.

In this paper we have performed an L + P analysis of our AA-PWA solution. Instead of using the whole energy range up to 2295 MeV, from our analysis we have omitted the high-energy part above 2179 MeV, where four spin observables Σ, T, $O_{x'}$, and $O_{z'}$ are not measured (cf. Table I) because we anticipate discontinuities in our solution in that energy range. Observe that this is also the energy range analyzed in Refs. [26,27]. The fit has been performed with two and three poles, and our solutions are documented in Fig. 17 and Table III.

In spite of obtaining a suspiciously narrow width of 33 MeV, the BG-SE solution is completely consistent with a $N(1880)\frac{1}{2}^+$ resonant state, and in Refs. [26,27] it has been interpreted as such. However, both our fits depicted in Figs. 17(b) and 17(c) do not support this conclusion. While the BG-SE fit identifies only a $N(1880)\frac{1}{2}^+$ state, our model clearly confirms the existence of $N(1710)\frac{1}{2}^+$ and $N(2100)\frac{1}{2}^+$ states, too. In Fig. 17(b) we show the fit of the data with two poles only. The fit is smooth and reliable, with $\chi^2 = 32$, and covers all data in the whole energy range very reliably. Some deviation from the data is only seen in the energy range of the $N(1880)\frac{1}{2}^+$ resonance, but it is small. In Fig. 17(c) we show the three-pole fit to the data. The χ^2 is slightly improved from 32 to 29.2, but the obtained resonance, in spite of being in the right place at 1882 MeV, has an extremely narrow width of 6 MeV.

As such a narrow state of 6 MeV is extremely unlikely, and we do not see the mechanism how a wider state could influence data in such a narrow energy range, we do not confirm the existence of $N(1880)\frac{1}{2}^+$ state contrary to Bonn-Gatchina result. We confirm that we do have a "one- or two-point structure," but as the energy step in BG-SE case is much wider (20 MeV) the width of the disturbance raises to ca 30 MeV. In our case our energy step is much lower (ca. 2–5 MeV), a two-point structure remains, but the width of a corresponding resonance becomes much narrower.

We conclude that L + P analysis indicates that the narrow disturbance in this energy range is more consistent with the instability due to violation of data consistency at this narrow energy range than to the existence of $N(1880)\frac{1}{2}^+$ resonance.

V. CONCLUSIONS AND OUTLOOK

The proposed single-channel, single-energy data analysis method AA-PWA, fully explained and demonstrated for η photoproduction in Ref. [22], has been applied to the world collection of data for $K\Lambda$ photoproduction. It is shown that a precise set of multipoles which improves the agreement with the data compared with the theoretical ED Bonn-Gatchina model [34] was obtained. Some discontinuities in the obtained multipoles are observed, and this is explained by the violation of self-consistency of the measured data, as well as the incompleteness of existing data sets. To overcome these difficulties a stronger constraint on the penalizing functions is required. Let us observe that, after *Step 1*, the constraining amplitudes can be discontinuous because their continuity is in the present AA-PWA method guaranteed only by data consistency and completeness of the data set. As both requirements are not met in most measured processes, additional conditions for the achievement of continuity are needed. One natural way is to impose fixed-t analyticity [18–20].

The obtained results were compared with the already published classic SE-PWA made in Refs. [26,27], and it has been shown that our results qualitatively and quantitatively agree with the results of these references. The mutual agreement of both approaches improves the probability that they are correct.

We confirm that the M_{1-} multipole in our model reproduces a narrow structure around 1880 MeV, but our L + P analysis fails to confirm that this structure is the confirmation of a $N(1880)\frac{1}{2}^+$ resonant state. The pole which would explain this structure in our model is much narrower than the anyways very narrow pole given in Refs. [26,27] (1876 MeV − i31 MeV), so we interpret it as a discontinuity due to data inconsistency rather than a resonance signal. Preliminary tests have confirmed that if we more strongly constrain the TPWA of the second step of the AA-PWA method to the smooth amplitudes of the ED BG2017 model, this structure disappears. However, this has to be elaborated in forthcoming presentations.

As the method shows a strong sensitivity to the self-consistency of the data, we advocate it as a reliable method to perform data self-consistency testing.

TABLE IV. The definitions of the 16 polarization observables of pseudoscalar meson photoproduction are given here in terms of transversity amplitudes $b_1, \ldots, b_4$ (cf. Ref. [52]; sign conventions are consistent with Ref. [56]). Expressions are given both in terms of real- and imaginary parts of bilinear products of amplitudes and in terms of moduli and relative phases of the amplitudes. Furthermore, the phase-space factor ρ has been suppressed in the given expressions (i.e., we have set $\rho = 1$). The four different groups of four observables each are indicated as well.

Observable	Group
$\sigma_0 = \frac{1}{2}(\lvert b_1\rvert^2 + \lvert b_2\rvert^2 + \lvert b_3\rvert^2 + \lvert b_4\rvert^2)$	
$\hat{\Sigma} = \frac{1}{2}(-\lvert b_1\rvert^2 - \lvert b_2\rvert^2 + \lvert b_3\rvert^2 + \lvert b_4\rvert^2)$	$\mathcal{S}$
$\hat{T} = \frac{1}{2}(\lvert b_1\rvert^2 - \lvert b_2\rvert^2 - \lvert b_3\rvert^2 + \lvert b_4\rvert^2)$	
$\hat{P} = \frac{1}{2}(-\lvert b_1\rvert^2 + \lvert b_2\rvert^2 - \lvert b_3\rvert^2 + \lvert b_4\rvert^2)$	
$\hat{E} = \mathrm{Re}[-b_3^* b_1 - b_4^* b_2] = -\lvert b_1\rvert\lvert b_3\rvert\cos\phi_{13} - \lvert b_2\rvert\lvert b_4\rvert\cos\phi_{24}$	
$\hat{F} = \mathrm{Im}[b_3^* b_1 - b_4^* b_2] = \lvert b_1\rvert\lvert b_3\rvert\sin\phi_{13} - \lvert b_2\rvert\lvert b_4\rvert\sin\phi_{24}$	$\mathcal{BT}$
$\hat{G} = \mathrm{Im}[-b_3^* b_1 - b_4^* b_2] = -\lvert b_1\rvert\lvert b_3\rvert\sin\phi_{13} - \lvert b_2\rvert\lvert b_4\rvert\sin\phi_{24}$	
$\hat{H} = \mathrm{Re}[b_3^* b_1 - b_4^* b_2] = \lvert b_1\rvert\lvert b_3\rvert\cos\phi_{13} - \lvert b_2\rvert\lvert b_4\rvert\cos\phi_{24}$	
$\hat{C}_{x'} = \mathrm{Im}[-b_4^* b_1 + b_3^* b_2] = -\lvert b_1\rvert\lvert b_4\rvert\sin\phi_{14} + \lvert b_2\rvert\lvert b_3\rvert\sin\phi_{23}$	
$\hat{C}_{z'} = \mathrm{Re}[-b_4^* b_1 - b_3^* b_2] = -\lvert b_1\rvert\lvert b_4\rvert\cos\phi_{14} - \lvert b_2\rvert\lvert b_3\rvert\cos\phi_{23}$	$\mathcal{BR}$
$\hat{O}_{x'} = \mathrm{Re}[-b_4^* b_1 + b_3^* b_2] = -\lvert b_1\rvert\lvert b_4\rvert\cos\phi_{14} + \lvert b_2\rvert\lvert b_3\rvert\cos\phi_{23}$	
$\hat{O}_{z'} = \mathrm{Im}[b_4^* b_1 + b_3^* b_2] = \lvert b_1\rvert\lvert b_4\rvert\sin\phi_{14} + \lvert b_2\rvert\lvert b_3\rvert\sin\phi_{23}$	
$\hat{L}_{x'} = \mathrm{Im}[-b_2^* b_1 - b_4^* b_3] = -\lvert b_1\rvert\lvert b_2\rvert\sin\phi_{12} - \lvert b_3\rvert\lvert b_4\rvert\sin\phi_{34}$	
$\hat{L}_{z'} = \mathrm{Re}[-b_2^* b_1 - b_4^* b_3] = -\lvert b_1\rvert\lvert b_2\rvert\cos\phi_{12} - \lvert b_3\rvert\lvert b_4\rvert\cos\phi_{34}$	$\mathcal{TR}$
$\hat{T}_{x'} = \mathrm{Re}[b_2^* b_1 - b_4^* b_3] = \lvert b_1\rvert\lvert b_2\rvert\cos\phi_{12} - \lvert b_3\rvert\lvert b_4\rvert\cos\phi_{34}$	
$\hat{T}_{z'} = \mathrm{Im}[-b_2^* b_1 + b_4^* b_3] = -\lvert b_1\rvert\lvert b_2\rvert\sin\phi_{12} + \lvert b_3\rvert\lvert b_4\rvert\sin\phi_{34}$	

ACKNOWLEDGMENTS

The work of Y.W. was funded by the Transdisciplinary Research Area Matter (University of Bonn) as part of the Excellence Strategy of the federal and state governments during the completion of this paper

APPENDIX A: GENERAL PHOTOPRODUCTION FORMALISM

In this Appendix, we collect essential parts of the general formalism for pseudoscalar meson photoproduction in order to keep the present work self-contained. We consider the following $2 \to 2$ reaction:

$$\gamma(p_\gamma; m_\gamma) + N(P_i; m_{s_i}) \longrightarrow K(p_K) + \Lambda(P_f; m_{s_f}). \quad \text{(A1)}$$

The 4-momenta as well as the variables necessary to label the spin-states have been indicated for each particle.

The photoproduction process is conventionally described using the well-known Mandelstam variables s, t, and u. Since 4-momentum conservation holds, i.e., $p_\gamma + P_i = p_K + P_f$, each of the Mandelstam variables can be written in two equivalent forms:

$$s = (p_\gamma + P_i)^2 = (p_K + P_f)^2, \quad \text{(A2)}$$

$$t = (p_\gamma - p_K)^2 = (P_f - P_i)^2, \quad \text{(A3)}$$

$$u = (p_\gamma - P_f)^2 = (P_i - p_K)^2. \quad \text{(A4)}$$

Since all particles in the initial- and final state of the reaction (A1) are assumed to be on the mass-shell, the whole reaction can be described by two independent kinematic invariants. The latter are often chosen to be the pair (s, t).

In this work, center-of-mass (CMS) coordinates are adopted. The following relations are valid between (s, t) and the center-of-mass energy W and scattering angle θ of the reaction:

$$s = W^2, \quad \text{(A5)}$$

$$t = m_K^2 - 2k\sqrt{m_K^2 + q^2} + 2kq\cos\theta. \quad \text{(A6)}$$

In these expressions, k and q are the absolute values of the CMS 3-momenta for the photon and the kaon, respectively. Both of these variables can be expressed in terms of W and the masses of the particles in the initial and final states. One can therefore describe the reaction equivalently in terms of (W, θ). The phase-space factor for the considered reaction (A1) is defined as $\rho = q/k$.

The general decomposition of the reaction amplitude into contributions of individual spin amplitudes has been found by Chew, Goldberger, Low, and Nambu (CGLN) [51] and it reads as follows:

$$\mathcal{F} = \chi^\dagger_{m_{s_f}} (i\vec{\sigma}\cdot\hat{\epsilon}\, F_1 + \vec{\sigma}\cdot\hat{q}\,\vec{\sigma}\cdot\hat{k}\times\hat{\epsilon}\, F_2 + i\vec{\sigma}\cdot\hat{k}\,\hat{q}\cdot\hat{\epsilon}\, F_3 + i\vec{\sigma}\cdot\hat{q}\,\hat{q}\cdot\hat{\epsilon}\, F_4)\,\chi_{m_{s_i}}. \quad \text{(A7)}$$

In this expression, $\hat{k}$ and $\hat{q}$ are normalized CMS 3-momenta, $\hat{\epsilon}$ is the normalized photon polarization vector and $\chi_{m_{s_i}}$, $\chi_{m_{s_f}}$ are Pauli spinors for the baryons in the initial and final states. The complex amplitudes $F_1, \ldots, F_4$ are called *CGLN amplitudes* and they depend on (W, θ). This set of four amplitudes contains the full information on the dynamics of the considered process (A1).

The so-called *transversity amplitudes* $b_1, \ldots, b_4$ are defined by rotating the spin-quantization axis away from the $\hat{z}$ axis of the CMS frame, which has been inherent to equation (A7), to the direction normal to the so-called reaction plane. The latter plane is spanned by the CMS 3-momenta $\vec{k}$ and $\vec{q}$. Using the conventions employed implicitly in the work of Chiang and Tabakin [52], one obtains the following set of linear and invertible relations between transversity and CGLN amplitudes (see also Ref. [53]):

$$b_1(W,\theta) = -b_3(W,\theta) - \frac{1}{\sqrt{2}}\sin\theta[F_3(W,\theta)e^{-i\frac{\theta}{2}} + F_4(W,\theta)e^{i\frac{\theta}{2}}], \quad \text{(A8)}$$

$$b_2(W,\theta) = -b_4(W,\theta) + \frac{1}{\sqrt{2}}\sin\theta[F_3(W,\theta)e^{i\frac{\theta}{2}} + F_4(W,\theta)e^{-i\frac{\theta}{2}}], \quad \text{(A9)}$$

$$b_3(W,\theta) = \frac{i}{\sqrt{2}}[F_1(W,\theta)e^{-i\frac{\theta}{2}} - F_2(W,\theta)e^{i\frac{\theta}{2}}], \tag{A10}$$

$$b_4(W,\theta) = \frac{i}{\sqrt{2}}[F_1(W,\theta)e^{i\frac{\theta}{2}} - F_2(W,\theta)e^{-i\frac{\theta}{2}}]. \tag{A11}$$

The transversity basis greatly simplifies the mathematical form of the definitions of the polarization observables (see Table IV and the discussion further below). For this reason, this basis is also used in the analysis performed in the present work (cf. Sec. III).

To access information on individual resonances, partial waves have to be analyzed. In the present work, we adopt the well-known expansion of the CGLN amplitudes into electric and magnetic multipoles $\{E_{\ell\pm}, M_{\ell\pm}\}$, i.e. [51,54],

$$F_1(W,\theta) = \sum_{\ell=0}^{\infty}\{[\ell M_{\ell+}(W) + E_{\ell+}(W)]P'_{\ell+1}(\cos\theta) + [(\ell+1)M_{\ell-}(W) + E_{\ell-}(W)]P'_{\ell-1}(\cos\theta)\}, \tag{A12}$$

$$F_2(W,\theta) = \sum_{\ell=1}^{\infty}[(\ell+1)M_{\ell+}(W) + \ell M_{\ell-}(W)]P'_{\ell}(\cos\theta), \tag{A13}$$

$$F_3(W,\theta) = \sum_{\ell=1}^{\infty}\{[E_{\ell+}(W) - M_{\ell+}(W)]P''_{\ell+1}(\cos\theta) + [E_{\ell-}(W) + M_{\ell-}(W)]P''_{\ell-1}(\cos\theta)\}, \tag{A14}$$

$$F_4(W,\theta) = \sum_{\ell=2}^{\infty}[M_{\ell+}(W) - E_{\ell+}(W) - M_{\ell-}(W) - E_{\ell-}(W)]P''_{\ell}(\cos\theta). \tag{A15}$$

The multipoles can be assigned to definite conserved spin-parity quantum numbers J^P (resonances with spin $J = |\ell \pm \frac{1}{2}|$ couple to the multipoles $E_{\ell\pm}$ and $M_{\ell\pm}$). The multipole expansion of the F_i can be formally inverted using a set of known projection integrals [55,56].

The polarization observables accessible in pseudoscalar meson photoproduction are dimensionless asymmetries among differential cross sections for different beam, target, and recoil polarization states:

$$\mathcal{O} = \frac{\beta\left[\left(\frac{d\sigma}{d\Omega}\right)^{(B_1,T_1,R_1)} - \left(\frac{d\sigma}{d\Omega}\right)^{(B_2,T_2,R_2)}\right]}{\sigma_0}. \tag{A16}$$

The factor β is a consistency factor introduced in Ref. [54]. It takes the value $\beta = \frac{1}{2}$ for observables which involve only beam and target polarization and $\beta = 1$ for quantities with recoil polarization. The unpolarized cross section σ_0 is always the sum of the two polarization configurations present in equation (A16): $\sigma_0 = \beta[(\frac{d\sigma}{d\Omega})^{(B_1,T_1,R_1)} + (\frac{d\sigma}{d\Omega})^{(B_2,T_2,R_2)}]$.

The dimensioned asymmetry $\sigma_0\mathcal{O}$ is often called a *profile function* [52,56] and is distinguished by a hat on the $\mathcal{O}$:

$$\hat{\mathcal{O}} = \beta\left[\left(\frac{d\sigma}{d\Omega}\right)^{(B_1,T_1,R_1)} - \left(\frac{d\sigma}{d\Omega}\right)^{(B_2,T_2,R_2)}\right]. \tag{A17}$$

For single-meson photoproduction, there exist in total 16 polarization observables [52,54]. They include the unpolarized cross section σ_0 and 15 further single- and double-polarization observables. The full set of 16 observables can be divided into the four groups of single-spin observables ($\mathcal{S}$), beam-target ($\mathcal{BT}$), beam-recoil ($\mathcal{BR}$), and target-recoil ($\mathcal{TR}$) observables [52]. Each group is composed of four quantities. The definitions of the 16 observables in terms of transversity amplitudes are given in Table IV.

APPENDIX B: SOLUTION-THEORY FOR THE COMPLETE-EXPERIMENT ANALYSIS OF THE INVESTIGATED DATABASE

In the following, we give some more mathematical details on the possible ambiguities of the complete-experiment analysis (CEA) when it is applied to the database analyzed in this work (cf. Sec. III A). We are well aware that the facts given below can be extracted from the well-known mathematical treatments in the CEA for photoproduction [52,57]. Still, we hope that the details given in the following can provide some intuition on the mathematical ambiguities one has to be careful about when analyzing the present database.

1. Lower-energy region (1625–2179 MeV): Observables $\{\sigma_0, \hat{\Sigma}, \hat{T}, \hat{P}, \hat{O}_{x'}, \hat{O}_{z'}, \hat{C}_{x'}, \hat{C}_{z'}\}$

We consider the definitions (cf. Table IV) of the eight analyzed observables (in the following, we set $\rho = q/k \equiv 1$):

$$\sigma_0 = \tfrac{1}{2}(|b_1|^2 + |b_2|^2 + |b_3|^2 + |b_4|^2), \tag{B1}$$

$$\hat{\Sigma} = \tfrac{1}{2}(-|b_1|^2 - |b_2|^2 + |b_3|^2 + |b_4|^2), \tag{B2}$$

$$\hat{T} = \tfrac{1}{2}(|b_1|^2 - |b_2|^2 - |b_3|^2 + |b_4|^2), \tag{B3}$$

$$\hat{P} = \tfrac{1}{2}(-|b_1|^2 + |b_2|^2 - |b_3|^2 + |b_4|^2), \tag{B4}$$

$$\hat{O}_{x'} = \mathrm{Re}[-b_1 b_4^* + b_2 b_3^*], \tag{B5}$$

$$\hat{O}_{z'} = \mathrm{Im}[b_1 b_4^* + b_2 b_3^*], \tag{B6}$$

$$\hat{C}_{x'} = \mathrm{Im}[-b_1 b_4^* + b_2 b_3^*], \tag{B7}$$

$$\hat{C}_{z'} = \mathrm{Re}[-b_1 b_4^* - b_2 b_3^*]. \tag{B8}$$

In case the phases of the transversity amplitudes $b_j = |b_j|e^{i\phi_j}$ are fixed to values coming from an energy-dependent, unitary PWA model (e.g., BnGa), one can see very quickly that the

system of equations composed of the eight observables (B1) to (B8) is in principle capable of fixing the four moduli $|b_i|$ uniquely. In fact, the group-$\mathcal{S}$ observables $\{\sigma_0, \hat{\Sigma}, \hat{T}, \hat{P}\}$ alone are already capable of that feat and the four additional observables only should make the solution more stable.

In case we also wish to determine the phases of the four transversity amplitudes, the situation is as follows: the four moduli $|b_i|$ are fixed uniquely by the group-$\mathcal{S}$ observables and the four additional observables $\{\hat{O}_{x'}, \hat{O}_{z'}, \hat{C}_{x'}, \hat{C}_{z'}\}$ can uniquely pin down the *relative phases* ϕ_{14} and ϕ_{23}. The latter statement is true due to the inverse relations:

$$e^{i\phi_{14}} = \frac{\mathrm{Re}[b_1 b_4^*] + i\mathrm{Im}[b_1 b_4^*]}{|b_1||b_4|} = \frac{(-\hat{O}_{x'} - \hat{C}_{z'}) + i(\hat{O}_{z'} - \hat{C}_{x'})}{2|b_1||b_4|}, \tag{B9}$$

$$e^{i\phi_{23}} = \frac{\mathrm{Re}[b_2 b_3^*] + i\mathrm{Im}[b_2 b_3^*]}{|b_2||b_3|} = \frac{(\hat{O}_{x'} - \hat{C}_{z'}) + i(\hat{O}_{z'} + \hat{C}_{x'})}{2|b_2||b_3|}. \tag{B10}$$

The complex exponential functions $e^{i\phi_{jk}}$ can be inverted uniquely for phases on the interval $\phi_{jk} \in [0, 2\pi)$ (via the arctan2 function).

The amplitude-arrangement of four transversity amplitudes is, however, not uniquely fixed.[7] One additional "connecting" relative phase is missing, for instance, ϕ_{12} or ϕ_{34}. In other words, the two subsets of amplitudes $\{b_1, b_4\}$ and $\{b_2, b_3\}$ can be rotated relative to each other in a *completely free way* and the observables $\{\hat{O}_{x'}, \hat{O}_{z'}, \hat{C}_{x'}, \hat{C}_{z'}\}$ are *completely blind to such a rotation*. As an example, consider a rotation of *only* the two amplitudes b_2 and b_3 by the same phase $\tilde{\varphi}$, which can have *any* dependence on energy and angle:

$$b_2(W,\theta) \longrightarrow e^{i\tilde{\varphi}(W,\theta)} b_2(W,\theta) \quad \text{and}$$
$$b_3(W,\theta) \longrightarrow e^{i\tilde{\varphi}(W,\theta)} b_3(W,\theta). \tag{B11}$$

This rotation leaves both relative phases ϕ_{14} and ϕ_{23} invariant and therefore also all four observables $\{\hat{O}_{x'}, \hat{O}_{z'}, \hat{C}_{x'}, \hat{C}_{z'}\}$. However, a rotation like (B11) generally leads to a new set of amplitudes with a very different partial-wave decomposition, since it changes the unknown continuum ambiguity phase (i.e., one overall phase for all four amplitudes) as well as the connecting relative phases ϕ_{12} and ϕ_{34}. One has to be careful about such effects when analyzing the data, although, as mentioned above, in our analysis this ambiguity is removed by fixing the phases of all four transversity amplitudes to a known ED model (cf. Secs. II and III).

2. Higher-energy region (2179–2296 MeV): Observables $\{\sigma_0, \hat{P}, \hat{C}_{x'}, \hat{C}_{z'}\}$

We start by considering the definitions (cf. Table IV) of the four analyzed observables (again setting $\rho = q/k \equiv 1$):

$$\sigma_0 = \tfrac{1}{2}(|b_1|^2 + |b_2|^2 + |b_3|^2 + |b_4|^2), \tag{B12}$$
$$\hat{P} = \tfrac{1}{2}(-|b_1|^2 + |b_2|^2 - |b_3|^2 + |b_4|^2), \tag{B13}$$
$$\hat{C}_{x'} = \mathrm{Im}[-b_1 b_4^* + b_2 b_3^*], \tag{B14}$$
$$\hat{C}_{z'} = \mathrm{Re}[-b_1 b_4^* - b_2 b_3^*]. \tag{B15}$$

We assume that the phases of the four transversity amplitudes are fixed to a model and define:

$$c_{ij} := \cos\phi_{ij} \quad \text{and} \quad s_{ij} := \sin\phi_{ij}. \tag{B16}$$

We reconsider the equations for $\hat{C}_{x'}$ and $\hat{C}_{z'}$:

$$\hat{C}_{x'} = -|b_1||b_4|s_{14} + |b_2||b_3|s_{23}, \tag{B17}$$
$$\hat{C}_{z'} = -|b_1||b_4|c_{14} - |b_2||b_3|c_{23}, \tag{B18}$$

and recognize that these equations can be inverted for the following products of moduli:

$$|b_1||b_4| = \frac{-c_{23}\hat{C}_{x'} - s_{23}\hat{C}_{z'}}{s_{14}c_{23} + c_{14}s_{23}} =: \xi_1, \tag{B19}$$
$$|b_2||b_3| = \frac{c_{14}\hat{C}_{x'} - s_{14}\hat{C}_{z'}}{s_{14}c_{23} + c_{14}s_{23}} =: \xi_2. \tag{B20}$$

The quantities ξ_1 and ξ_2 are uniquely fixed from the observables and the employed model phases.

We could now choose to eliminate, for instance, the quantities $|b_3|$ and $|b_4|$ in the equations for the cross section (B12) and the observable $\hat{P}$ (B13) and thus obtain

$$\sigma_0 = \frac{1}{2}\left[|b_1|^2 + |b_2|^2 + \left(\frac{\xi_2}{|b_2|}\right)^2 + \left(\frac{\xi_1}{|b_1|}\right)^2\right], \tag{B21}$$
$$\hat{P} = \frac{1}{2}\left[-|b_1|^2 + |b_2|^2 - \left(\frac{\xi_2}{|b_2|}\right)^2 + \left(\frac{\xi_1}{|b_1|}\right)^2\right]. \tag{B22}$$

These are two quadratic equations for the two remaining unknowns $|b_1|$ and $|b_2|$. One can make the following attempt at solving them: We multiply the equation (B22) by $|b_2|^2$ in order to obtain

$$|b_2|^4 + \left[\left(\frac{\xi_1}{|b_1|}\right)^2 - |b_1|^2 - 2\hat{P}\right]|b_2|^2 - (\xi_2)^2 = 0. \tag{B23}$$

This is a quadratic equation for $|b_2|^2$ and thus allows for the following two solutions:

$$|b_2|^2_{\mathrm{I,II}} = \frac{1}{2}\left[2\hat{P} + |b_1|^2 - \left(\frac{\xi_1}{|b_1|}\right)^2\right] \pm \sqrt{\frac{1}{4}\left[2\hat{P} + |b_1|^2 - \left(\frac{\xi_1}{|b_1|}\right)^2\right]^2 + (\xi_2)^2}. \tag{B24}$$

Irrespective of whether solution I or II is the correct one, the "+" branch of the square root has to be taken in order to arrive at a positive modulus $|b_2|$. In case both solutions I or II are allowed (i.e., larger than zero) in Eq. (B24), one obtains two permissible moduli $|b_2|_{\mathrm{I}}$ and $|b_2|_{\mathrm{II}}$. Then, one has to substitute these solutions into the equation for the cross section (B21) and solve for $|b_1|$. In this way, at most a set of four discrete ambiguities can emerge and all continuous ambiguities are resolved for the four moduli $|b_1|, \ldots, |b_4|$.

Therefore, in case one would attempt to let all four moduli $|b_1|, \ldots, |b_4|$ run freely in the AA step (i.e., our *Step 1*), we expect the found solution to lie on a well-defined (approximately) parabolic minimum where the derivative of the minimized ("χ^2-like") function exactly vanishes. Data for

[7] That is, uniquely up to one overall phase for *all* four amplitudes.

the four observables $\{\sigma_0, \hat{P}, \hat{C}_{x'}, \hat{C}_{z'}\}$ are, in principle, only capable of distinguishing solutions up to the above-mentioned discrete ambiguity. However, in case the initial conditions are well chosen for the minimization procedure, we are confident that the correct minimum can be found, i.e., that the moduli extraction is sufficiently stable.

[1] A. Martin and J.-M. Richard, Phys. Rev. D **101**, 094014 (2020).
[2] I. S. Stefanescu, Phys. Rev. D **21**, 3225 (1980); I. S. Stefanescu, Fortschr. Phys. **35**, 573 (1987).
[3] D. Atkinson, P. W. Johnson, and R. L. Warnock, Commun. Math. Phys. **33**, 221 (1973); J. E. Bowcock and H. Burkhard, Rep. Prog. Phys. **38**, 1099 (1975); D. Atkinson and I. S. Stefanescu, Commun. Math. Phys. **101**, 291 (1985).
[4] A. Švarc, Phys. Rev. C **104**, 014605 (2021).
[5] T. Mart and A. Sulaksono, Phys. Rev. C **74**, 055203 (2006).
[6] H. Kamano, S. X. Nakamura, T.-S. H. Lee, and T. Sato, Phys. Rev. C **88**, 035209 (2013).
[7] H. Kamano, T. S. H. Lee, S. X. Nakamura, and T. Sato, arXiv:1909.11935 [nucl-th].
[8] H. Kamano, S. X. Nakamura, T. S. H. Lee, and T. Sato, Phys. Rev. C **94**, 015201 (2016).
[9] A. V. Anisovich, R. Beck, E. Klempt, V. A. Nikonov, A. V. Sarantsev, and U. Thoma, Eur. Phys. J. A **48**, 15 (2012).
[10] A. V. Anisovich, R. Beck, M. Döring, M. Gottschall, J. Hartmann, V. Kashevarov, E. Klempt, U. G. Meißner, V. Nikonov, and M. Ostrick *et al.* Eur. Phys. J. A **52**, 284 (2016).
[11] D. Rönchen, M. Döring, F. Huang, H. Haberzettl, J. Haidenbauer, C. Hanhart, S. Krewald, U. G. Meißner, and K. Nakayama, Eur. Phys. J. A **49**, 44 (2013).
[12] D. Rönchen, M. Döring, and U. G. Meißner, Eur. Phys. J. A **54**, 110 (2018).
[13] B. C. Hunt and D. M. Manley, Phys. Rev. C **99**, 055204 (2019).
[14] B. C. Hunt and D. M. Manley, Phys. Rev. C **99**, 055203 (2019).
[15] B. C. Hunt and D. M. Manley, Phys. Rev. C **99**, 055205 (2019).
[16] R. L. Workman, R. A. Arndt, W. J. Briscoe, M. W. Paris, and I. I. Strakovsky, Phys. Rev. C **86**, 035202 (2012).
[17] R. G. Newton, J. Math. Phys. **9**, 2050 (1968).
[18] G. Höhler, *Pion Nucleon Scattering, Part 2, Landolt-Bornstein: Elastic and Charge Exchange Scattering of Elementary Particles* (Springer-Verlag, Berlin, 1983), Vol. 9b.
[19] H. Osmanović, M. Hadžimehmedović, R. Omerović, J. Stahov, M. Gorchtein, V. Kashevarov, K. Nikonov, M. Ostrick, L. Tiator, and A. Švarc, Phys. Rev. C **100**, 055203 (2019).
[20] H. Osmanović, M. Hadžimehmedović, R. Omerović, J. Stahov, V. Kashevarov, M. Ostrick, L. Tiator, and A. Švarc, Phys. Rev. C **104**, 034605 (2021).
[21] K. M. Watson, Phys. Rev. **95**, 228 (1954).
[22] A. Švarc, Y. Wunderlich, and L. Tiator, Phys. Rev. C **102**, 064609 (2020).
[23] A. Švarc, Y. Wunderlich, H. Osmanović, M. Hadžimehmedović, R. Omerović, J. Stahov, V. Kashevarov, K. Nikonov, M. Ostrick, L. Tiator, and R. Workman, Few-Body Syst. **59**, 96 (2018).
[24] V. L. Kashevarov, L. Tiator, and M. Ostrick, Bled Workshops Phys. **16**, 1 (2015).
[25] https://pwa.hiskp.uni-bonn.de/
[26] A. V. Anisovich, V. Burkert, M. Hadžimehmedović, D. G. Ireland, E. Klempt, V. A. Nikonov, R. Omerović, H. Osmanović, A. V. Sarantsev, J. Stahov, A. Švarc, and U. Thoma, Phys. Rev. Lett. **119**, 062004 (2017).
[27] A. V. Anisovich, V. Burkert, M. Hadžimehmedović, D. G. Ireland, E. Klempt, V. A. Nikonov, R. Omerović, H. Osmanović, A. V. Sarantsev, J. Stahov, A. Švarc, and U. Thoma, Eur. Phys. J. A **53**, 242 (2017).
[28] H. Osmanović, M. Hadžimehmedović, R. Omerović, J. Stahov, V. Kashevarov, K. Nikonov, M. Ostrick, L. Tiator, and A. Švarc, Phys. Rev. C **97**, 015207 (2018).
[29] A. Švarc, Y. Wunderlich, H. Osmanović, M. Hadžimehmedović, R. Omerović, J. Stahov, V. Kashevarov, K. Nikonov, M. Ostrich, L. Tiator, and R. Workman, Phys. Rev. C **97**, 054611 (2018).
[30] A. V. Anisovich, V. Burkert, N. Compton, K. Hicks, F. J. Klein, E. Klempt, V. A. Nikonov, A. M. Sandorfi, A. V. Sarantsev, and U. Thoma, Phys. Rev. C **96**, 055202 (2017).
[31] D. Rönchen, M. Döring, H. Haberzettl, J. Haidenbauer, U.-G. Meißner, and K. Nakayama, Eur. Phys. J. A **51**, 70 (2015).
[32] D. Drechsel, S. S. Kamalov, and L. Tiator, Eur. Phys. J. A **34**, 69 (2007);
[33] https://gwdac.phys.gwu.edu/.
[34] A. V. Anisovich (private communication).
[35] R. Bradford *et al.*, Phys. Rev. C **73**, 035202 (2006).
[36] M. E. McCracken *et al.*, Phys. Rev. C **81**, 025201 (2010).
[37] A. Lleres *et al.*, Eur. Phys. J. A **31**, 79 (2007).
[38] C. A. Paterson *et al.*, Phys. Rev. C **93**, 065201 (2016).
[39] Wolfram Research, Inc., *Mathematica*, Version 11.0, Champaign, IL, USA (2016).
[40] A. Švarc, M. Hadžimehmedović, H. Osmanović, J. Stahov, and R. L. Workman, Phys. Rev. C **91**, 015207 (2015).
[41] A. Švarc, M. Hadžimehmedović, H. Osmanović, J. Stahov, L. Tiator, and R. L. Workman, Phys. Rev. C **88**, 035206 (2013).
[42] A. Švarc, M. Hadžimehmedović, R. Omerović, H. Osmanović, and J. Stahov, Phys. Rev. C **89**, 045205 (2014).
[43] A. Švarc, M. Hadžimehmedović, H. Osmanović, J. Stahov, L. Tiator, and R. L. Workman, Phys. Rev. C **89**, 065208 (2014).
[44] P. A. Zyla *et al.* (Particle Data Group), Prog. Theor. Exp. Phys. **2020**, 083C01 (2020).
[45] S. Ciulli and J. Fischer, Nucl. Phys. **24**, 465 (1961).
[46] I. Ciulli, S. Ciulli, and J. Fisher, Nuovo Cimento **23**, 1129 (1962).
[47] E. Pietarinen, Nuovo Cimento A **12**, 522 (1972).
[48] E. Pietarinen, Nucl. Phys. B **107**, 21 (1976).
[49] M. Hazewinkel, *Encyclopaedia of Mathematics* (Springer, 1990), Vol. 6, p. 251.
[50] A. Švarc, M. Hadžimehmedović, H. Osmanović, J. Stahov, L. Tiator, and R. L. Workman, Phys. Lett. B **755**, 452 (2016).
[51] G. F. Chew, M. Goldberger, F. E. Low, and Y. Nambu, Phys. Rev. **106**, 1345 (1957).
[52] W. T. Chiang and F. Tabakin, Phys. Rev. C **55**, 2054 (1997).
[53] Y. Wunderlich, R. Beck, and L. Tiator, Phys. Rev. C **89**, 055203 (2014).
[54] A. M. Sandorfi, S. Hoblit, H. Kamano, and T.-S. H. Lee, J. Phys. G **38**, 053001 (2011).
[55] J. S. Ball, Phys. Rev. **124**, 2014 (1961).
[56] Y. Wunderlich, Ph.D. thesis, University of Bonn, 2019, arXiv:2008.00514 [nucl-th].
[57] K. Nakayama, Phys. Rev. C **100**, 035208 (2019).